CELLULAR NEUROSCIENCE

Loss of IRF2BPL impairs neuronal maintenance through excess Wnt signaling

Paul C. Marcogliese[1,2]*†, Debdeep Dutta[1,2]†, Shrestha Sinha Ray[3], Nghi D. P. Dang[4], Zhongyuan Zuo[1,2], Yuchun Wang[1,2], Di Lu[1,2], Fatima Fazal[1,2], Thomas A. Ravenscroft[1,2], Hyunglok Chung[1,2], Oguz Kanca[1,2], JiJun Wan[5], Emilie D. Douine[5], Undiagnosed Diseases Network, Loren D. M. Pena[6,7], Shinya Yamamoto[1,2,8,9,10], Stanley F. Nelson[5], Matthew Might[11], Kathrin C. Meyer[3,12], Nan Cher Yeo[4,11], Hugo J. Bellen[1,2,9]*

De novo truncations in *Interferon Regulatory Factor 2 Binding Protein Like* (*IRF2BPL*) lead to severe childhood-onset neurodegenerative disorders. To determine how loss of *IRF2BPL* causes neural dysfunction, we examined its function in *Drosophila* and zebrafish. Overexpression of either *IRF2BPL* or *Pits*, the *Drosophila* ortholog, represses Wnt transcription in flies. In contrast, neuronal depletion of Pits leads to increased *wingless* (*wg*) levels in the brain and is associated with axonal loss, whereas inhibition of Wg signaling is neuroprotective. Moreover, increased neuronal expression of *wg* in flies is sufficient to cause age-dependent axonal loss, similar to reduction of Pits. Loss of *irf2bpl* in zebrafish also causes neurological defects with an associated increase in *wnt1* transcription and downstream signaling. *WNT1* is also increased in patient-derived astrocytes, and pharmacological inhibition of Wnt suppresses the neurological phenotypes. Last, IRF2BPL and the Wnt antagonist, CKIα, physically and genetically interact, showing that IRF2BPL and CKIα antagonize Wnt transcription and signaling.

INTRODUCTION

We and others recently identified de novo truncating mutations in *Interferon Regulatory Factor 2 Binding Protein Like* (*IRF2BPL*) as the cause of a severe pediatric-onset neurological disorder termed NEDAMSS (neurodevelopmental disorder with regression, abnormal movements, loss of speech, and seizures; MIM #618088) (*1*, *2*). IRF2BP protein family members including IRF2BP1, IRF2BP2, and IRF2BPL contain a highly conserved coiled-coil DNA binding domain (IRF2BP zinc finger domain) at the N terminus and a C3HC4-type RING finger domain at the C terminus connected by a variable low-complexity region (*3*). The single *Drosophila* ortholog of the three vertebrate IRF2BP family members is Pits (protein interacting with Ttk69 and Sin3A) (*4*). *Pits* is an essential gene whose loss causes embryonic lethality (*1*). The Pits protein is detected primarily in the nucleus of most neurons in the adult fly brain, and its neuronal knockdown leads to behavioral defects (*1*).

It is unclear how loss of Pits/IRF2BPL leads to neurological dysfunction. Here, we show that overexpression of human *IRF2BPL* and *Drosophila Pits* in the fly wing imaginal disc causes a phenotype that is typically associated with loss of Wnt (Wingless/Integrated) signaling. The Wnt family of ligands including Wingless (Wg; WNT1 ortholog in *Drosophila*) are critical glycoproteins, secreted as morphogens, and are key regulators of development (*5*–*7*). Alterations in Wnt signaling components are associated with skeletal disorders, cancers (particularly colorectal cancer), and some neurological diseases (*8*, *9*). In the developing nervous system, Wnt has a critical role in regulating cell proliferation, migration, differentiation, and synapse development (*10*). However, the role of Wnt signaling in the adult brain is ill-defined. Most Wnt signaling components are expressed in the adult mouse brain (*11*), and Wnt signaling has been shown to modulate synaptic plasticity (*12*). While altered Wnt signaling, both increased and decreased, has been implicated in some neurological disorders and decreased Wnt signaling has been associated with neurodegeneration (*9*), a link between up-regulated Wnt signaling and neurodegeneration has not been identified.

We investigated the relationship between Pits/IRF2BPL and Wnt in *Drosophila*, zebrafish, and NEDAMSS patient cells. We report that neuronal reduction of Pits increases *wg* transcript levels, resulting in progressive axonal degeneration. Conversely, overexpression of *Pits* or human *IRF2BPL* leads to a reduction of *wg* transcription. Neuronal overexpression of Wg mimics the Pits loss-of-function phenotypes in flies. Zebrafish lacking *irf2bpl* display neurobehavioral defects, and drugs that inhibit Wnt signaling suppress the phenotypes associated with loss of Pits or Irf2bpl in flies and fish. Human IRF2BPL and *Drosophila* Pits share conserved physical and genetic interactions with the Wg/Wnt destruction complex component, CKIα. Last, NEDAMSS patient skin fibroblast-derived astrocytes produce excess *WNT1*. In summary, our data show that protracted up-regulation of Wnt transcription in the nervous system occurs when IRF2BPL is down-regulated, and is detrimental for the long-term maintenance and function of neurons.

RESULTS

Pits and IRF2BPL inhibit *wingless* transcription and signaling

Overexpression of *IRF2BPL* or *Pits*, either ubiquitously (*Actin[Act]-GAL4*) or using a *Pits*-specific driver ($Pits^{TG4}$, a *GAL4* insertion in

[1]Department of Molecular and Human Genetics, Baylor College of Medicine, Houston, TX 77030, USA. [2]Jan and Dan Duncan Neurological Research Institute, Texas Children's Hospital, Houston, TX 77030, USA. [3]The Research Institute at Nationwide Children's Hospital, Columbus, OH 43205, USA. [4]Department of Pharmacology and Toxicology, University of Alabama, Birmingham, AL 35294, USA. [5]Department of Human Genetics, David Geffen School of Medicine at UCLA, Los Angeles, CA 90095, USA. [6]Division of Human Genetics, Cincinnati Children's Hospital Medical Center, Cincinnati, OH 45229, USA. [7]Department of Pediatrics, University of Cincinnati College of Medicine, Cincinnati, OH 45267, USA. [8]Program in Developmental Biology, Baylor College of Medicine, Houston, TX 77030, USA. [9]Department of Neuroscience, Baylor College of Medicine, Houston, TX 77030, USA. [10]Development, Disease Models & Therapeutics Graduate Program, Baylor College of Medicine, Houston, TX 77030, USA. [11]Precision Medicine Institute, University of Alabama, Birmingham, AL 35294, USA. [12]Department of Pediatrics, The Ohio State University, Columbus, OH 43210, USA.
*Corresponding author. Email: hbellen@bcm.edu (H.J.B.); paul.c.marcogliese@gmail.com (P.C.M.)
†These authors contributed equally to this work.

Pits), causes lethality in flies (*1*). Moreover, *IRF2BPL* expression in the developing wing pouch, using *nubbin(nub)-GAL4*, also causes lethality at 25°C (*13*). We therefore reduced the overexpression levels of *IRF2BPL* and *Pits* driven in the wing pouch by incubating flies at 18°C. These flies (*nub-GAL4, UAS-IRF2BPL* or *nub-GAL4, UAS-Pits*) are viable but display a highly penetrant wing margin loss (Fig. 1A and fig. S1A) at the anterior (red arrows) and posterior margin (green arrows). These data indicate that IRF2BPL and Pits share similar functions in this context.

Bristle loss and serration of the wing are commonly observed upon disruption of the Wnt signaling pathway (*14*). We therefore examined components of the Wnt pathway (Fig. 1B) in the developing wing disc of third instar larvae upon expression of *IRF2BPL* in the wing pouch. We found that wing-specific expression of full-length human *IRF2BPL* leads to a loss of Wg protein in both anterior (cyan arrow) and posterior (yellow arrow) regions of the dorsal-ventral (DV) boundary that correspond to the affected areas we observed in the adult wing margin (Fig. 1C). Moreover, expression of

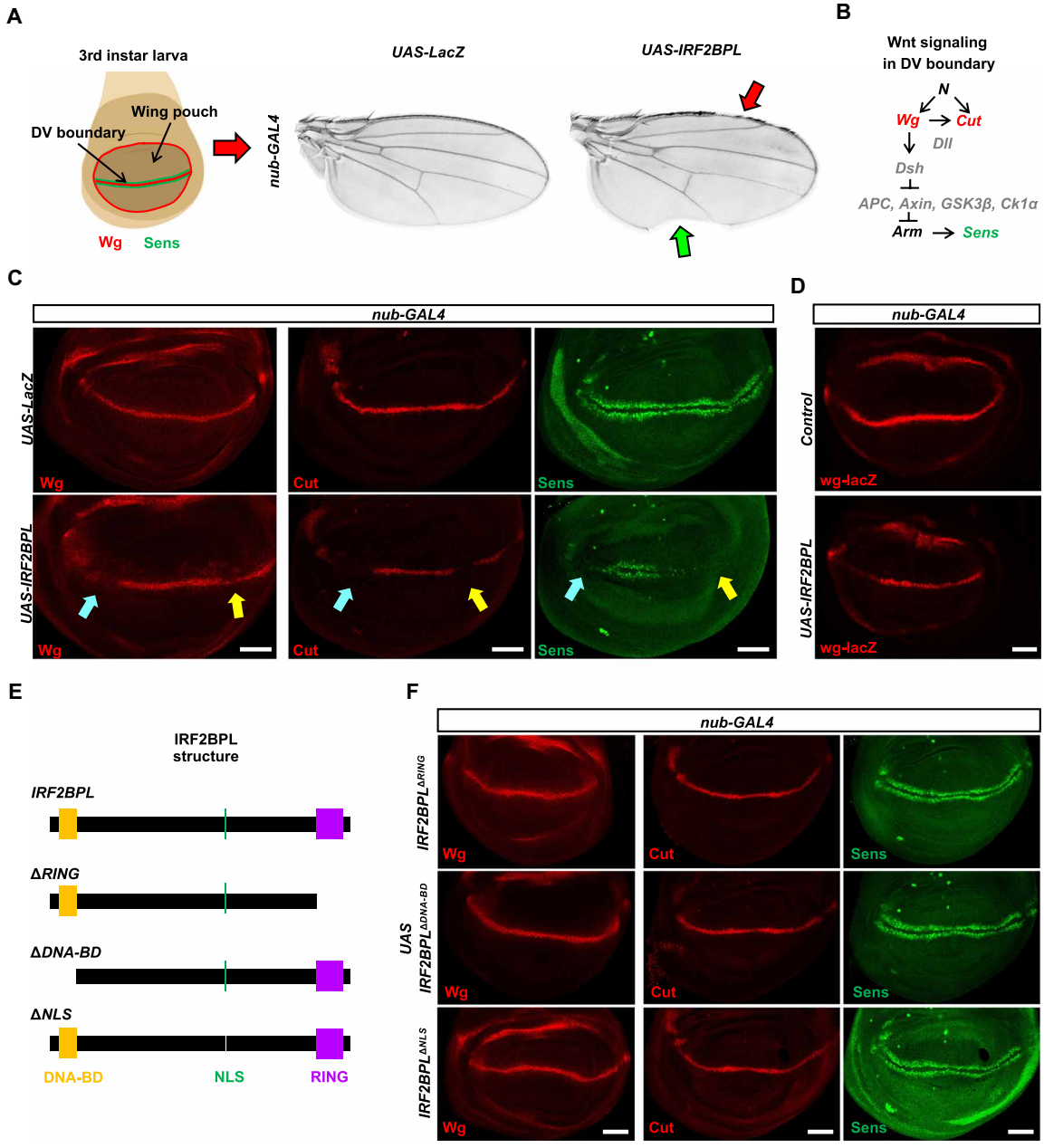

Fig. 1. IRF2BPL overexpression decreases *wg* transcript, protein, and signaling in the wing disc. (**A**) Schematic of the developing wing pouch where the Wg expression along the DV boundary develops into the adult wing margin. Optical images of the adult fly wing upon overexpression of *UAS-LacZ* or *UAS-IRF2BPL* constructs with *nub-GAL4* at 18°C. (**B**) Wnt pathway in the developing wing pouch at the DV boundary. (**C** and **D**) Third instar larval wing disc upon overexpression of *UAS-LacZ* or *UAS-IRF2BPL* with *nub-GAL4* at 18°C and stained with anti-Wg or Wnt downstream targets anti-Cut and anti-Sens (C) or the *wg-lacZ* reporter gene (D). Note the absence of Wg or its downstream responders by the arrows. (**E**) IRF2BPL protein structure and schematic of deletion constructs. (**F**) Third instar larval wing disc upon overexpression of *UAS-IRF2BPL* constructs with nub-GAL4 at 18°C and stained with anti-Wg or Wnt downstream targets anti-Cut and anti-Sens. Scale bars, 40 μm.

IRF2BPL in the developing wing leads to decreased levels of Cut (*15*), as well as the Wg-responsive transcription factor Senseless (Sens) (*16*) (Fig. 1C). To determine whether *IRF2BPL* expression affects *wg* transcription, we used a *wg-lacZ* reporter gene. We observed decreased *wg-lacZ* signal upon overexpression of IRF2BPL (Fig. 1D). Together, the above data indicate that full-length IRF2BPL decreases *wg* transcription and protein levels, and its downstream signaling components lead to bristle loss and serration in the adult wing.

To determine the signatures within IRF2BPL that are required for its ability to inhibit *wg*, we removed the DNA binding domain (Δ*DNA-BD*), RING domain (Δ*RING*), and the KRK nuclear localization signal (Δ*NLS*) in IRF2BPL (Fig. 1E). We expressed these constructs in the developing wing pouch with *nub-GAL4* at 18°C. As shown in Fig. 1F, both conserved domains and the NLS are required for inhibition of Wg in the DV boundary and fail to produce any adult wing margin phenotype (Fig. 1F and fig. S1, B to E). Moreover, wing-specific expression of either the IRF2BPL DNA-BD or the RING domain alone is not sufficient to cause a wing phenotype in flies (fig. S1F). In summary, both conserved DNA binding and RING domains and proper nuclear localization of Pits and IRF2BPL are all required to inhibit Wg in vivo.

Neuronal Pits is required for normal life span, behavior, and axonal integrity

To assess the role of Pits in neurons, we generated an internally tagged green fluorescent protein (GFP) trap allele (*Pits::GFP^{DH}*) (Fig. 2A) (*1*, *17*). Unlike *Pits* loss-of-function mutants that are homozygous lethal (*1*), the GFP-tagged *Pits* gene does not disrupt protein function as homozygous *Pits::GFP^{DH}* flies are viable and display no obvious phenotype. We used the deGradFP (*UAS-NSlmb::vhhGFP4*) strategy (*18*–*20*) that allows for the selective and reversible degradation of GFP-tagged proteins (Fig. 2B). The reduction of the GFP-tagged protein can be spatially controlled by the expression of *UAS-NSlmb::vhhGFP4* with specific GAL4 drivers. Conditional protein degradation is achieved by shifting the animals from lower to higher temperatures (from 18° to 29°C), taking advantage of the temperature sensitiveness of the UAS/GAL4 system (fig. S2A) (*19*). The constitutive reduction of Pits::GFP^{DH}, either ubiquitously (*Act-GAL4*) (Fig. 2C) or in neurons (*neuronal Synaptobrevin [nSyb]-GAL4*) (Fig. 2D), results in a life-span reduction when compared with control flies, which contain a non–GFP-tagged *Pits*-specific P[acman] 20-kb BAC (bacterial artificial chromosome)–based genomic rescue (GR) construct (*1*, *21*, *22*). In addition, we observed age-dependent climbing defects upon constitutive neuronal degradation of Pits::GFP^{DH}. Young flies at 5 days post-eclosion (d.p.e.) display normal climbing behavior, while aged flies with reduced Pits at 25 d.p.e. require significantly longer times to climb (Fig. 2E).

To explore the cellular effect of Pits reduction in neurons, we examined the integrity of the peripheral neurons of the anterior wing by performing transmission electron microscopy of the wing nerves of *Pits::GFP^{DH}; nSyb-GAL4, UAS-deGradFP* flies (Fig. 2F) (*23*, *24*). We did not detect any difference in axonal number or any obvious morphological changes in young animals (5 d.p.e.) upon constitutive Pits::GFP^{DH} degradation in neurons (Fig. 2G). However, we observed notable axonal loss in aged flies (25 d.p.e.) upon neuronal degradation of Pits::GFP^{DH} when compared to age-matched controls (Fig. 2H). Hence, the constitutive reduction of Pits in neurons leads to life-span deficits and progressive neural dysfunction associated with an age-dependent axonal loss.

To assess the consequences of the adult-specific reduction of Pits, we switched flies from 18° to 29°C upon eclosion to induce Pits degradation in adult flies using deGradFP. Adult-specific expression of deGradFP results in ~50 to 60% reduction in Pits::GFP^{DH} levels (fig. S2, A and B). We found that adult-specific degradation of Pits::GFP^{DH}, either ubiquitously or in neurons, results in reduced life span and progressive climbing defects (fig. S2, C to F). Furthermore, adult-specific reduction of Pits::GFP^{DH} using *Act-GAL4* results in axonal loss in the wing nerve (fig. S2G). In addition, we were able to prevent climbing defects at 25 d.p.e. by switching flies back to 18°C after incubating the flies for the first 12 days at 29°C (fig. S3, A to C). Together, these data indicate that adult-specific reduction of Pits is sufficient to cause decreased life span, as well as progressive neuronal dysfunction and axonal loss. Furthermore, a protracted period of time with Pits down-regulated is required to cause a slow and progressive loss of neural function.

IRF2BPL and *wingless* act antagonistically

To explore the functional antagonism between IRF2BPL and Wg, we coexpressed *UAS-IRF2BPL* and *UAS-Wg::HA* (*25*) in the developing wing pouch. We found that coexpression of *IRF2BPL* and *Wg* both dampens Wg protein levels and restores the DV boundary of the wing disc (Fig. 3A). Since this experiment requires two UAS constructs and one GAL4 driver, we coexpressed *UAS-IRF2BPL* with *UAS-LacZ* to avoid any dilution effects, as a control. In the adult wings, coexpression of *IRF2BPL* and *LacZ* leads to wing margin loss (>95% penetrant). However, the simultaneous overexpression of *IRF2BPL* and *Wg* results in normal wings in all flies (Fig. 3B). In agreement with the observed IRF2BPL and Wg antagonism, overexpression of *UAS-Wg::HA* with *nub-GAL4* at 18°C is pupal lethal, while coexpression of *UAS-Wg::HA* with *UAS-IRF2BPL* results in viable flies with normal wings. These data suggest a strong antagonistic relationship between the two proteins. To further determine whether IRF2BPL can act downstream of Wg expression, we overexpressed dishevelled (Dsh), known to cause redistribution and accumulation of β-catenin as a positive regulator of Wnt signaling (*26*). Ectopic expression of Dsh in the developing wing pouch causes wing blisters and ectopic bristles (fig. S4A). Coexpression of IRF2BPL with Dsh partially suppresses both the blister and bristle phenotypes (fig. S4, B and C). Moreover, *nub-GAL4*, *UAS,IRF2BPL*, *UAS-Dsh* flies do not exhibit the anterior bristle loss or wing serration associated with IRF2BPL expression in the wing. These data indicate an antagonistic genetic relationship of IRF2BPL with Dsh, suggesting that IRF2BPL can act downstream of Dsh.

Neuronal reduction of Pits increases Wg protein levels in the adult *Drosophila* CNS

Wnt signaling components, as well as Wnt ligands, are expressed in adult neurons (*27*). Since *Pits*/*IRF2BPL* overexpression leads to decreased *wg* in the wing imaginal disc, we determined whether reduction of Pits in neurons results in excess *wg* levels in the adult brain. We knocked down *Pits* mRNA in neurons using *elav-GAL4, UAS-Dicer* and an effective RNA interference (RNAi) transgene (*UAS-Pits-IR*) (*1*) and examined *wg* transcript and protein levels in fly heads. We found an increase in *wg* transcription (Fig. 3C and fig. S4D) and Wg protein (Fig. 3, D and E) in fly heads upon neuronal knockdown of *Pits* when compared to control RNAi targeting *luciferase* (*UAS-luc-IR*). Immunohistochemical staining of Wg in these brains also revealed a wider distribution of Wg protein upon

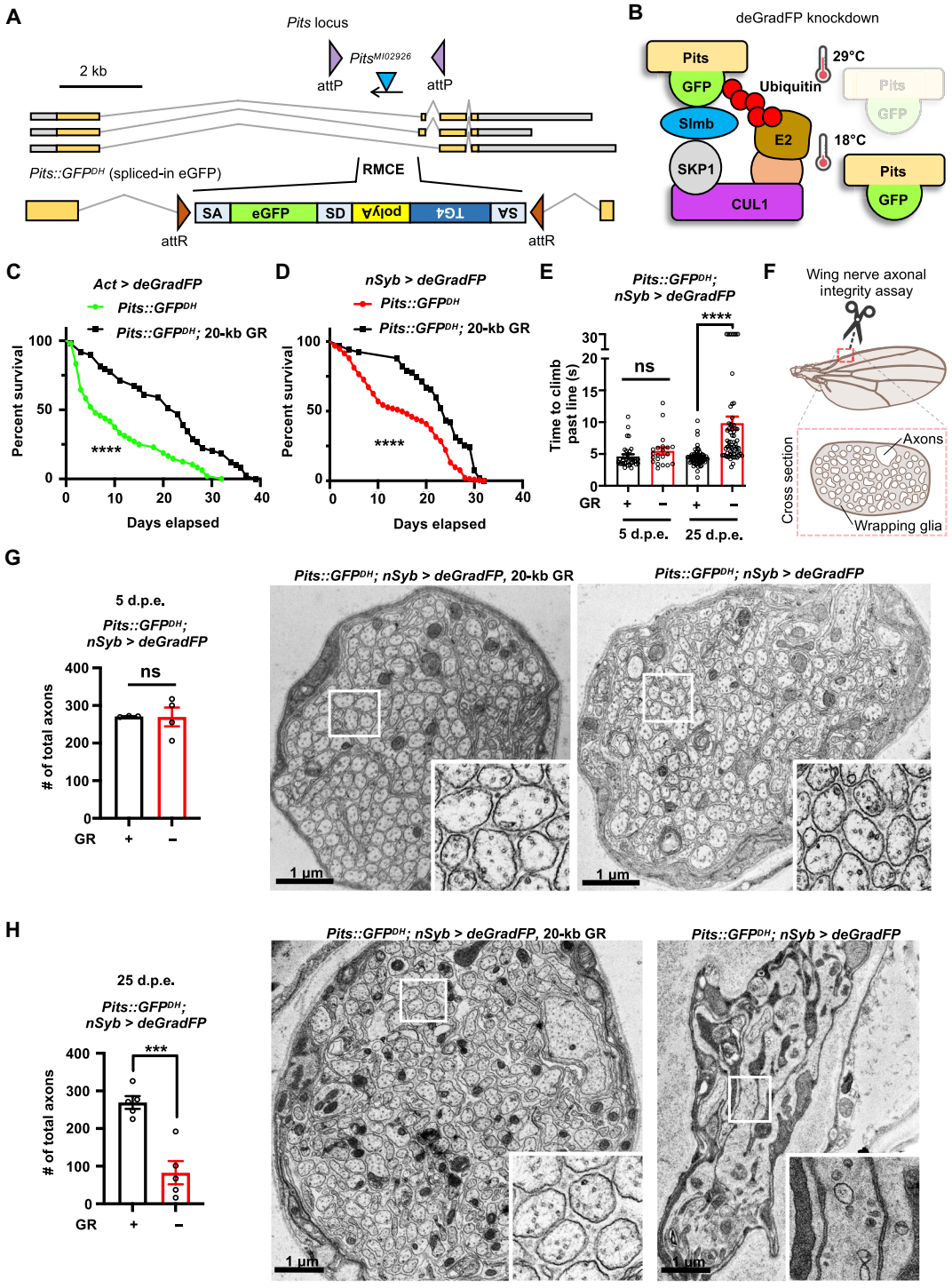

Fig. 2. Neuronal reduction of Pits reduces life span and causes progressive climbing defects and axonal loss. (**A**) Schematic of Pits locus in *Drosophila* with original *Pits*^{MI02926} insertion that was converted to *Pits::GFP*^{DH} by injection of Double Header plasmid (*20*), resulting in an internally tagged protein trap allele that affects all known Pits transcripts. (**B**) GFP-tagged fusion proteins can be targeted by deGradFP (*UAS-NSlmb::vhhGFP4*) to degrade Pits::GFP^{DH} with spatial (GAL4) and temporal (temperature) control. (**C** and **D**) Life span is decreased when Pits::GFP^{DH} is ubiquitously (C) or neuronally (D) degraded by deGradFP during development and the adult stage. *n* is a minimum of 48 flies per genotype (****$P < 0.0001$). Statistical analyses were determined by the log-rank test. (**E**) *Pits::GFP*^{DH}*; nSyb-GAL4, UAS-deGradFP* flies exhibit progressive climbing defects. Time (seconds) required for flies of the indicated genotypes to climb past 7 cm ($n > 20$ per genotype). Statistical analyses are one-way ANOVA followed by a Tukey post hoc test. Results are means ± SEM (****$P < 0.0001$). (**F** and **H**) Diagram of the peripheral wing nerves containing peripheral neurons of the anterior wing margin observed with (**G** and H) transmission electron microscopy. Quantification shows the total axon number at (G) 5 d.p.e. in *Pits::GFP*^{DH}*; nSyb-GAL4, UAS-deGradFP* flies containing GR construct ($n = 3$) and flies without GR ($n = 4$) and (H) 25 d.p.e. ($n = 5$ each genotype). Results are means ± SEM (***$P < 0.001$). Statistical analyses were determined by two-tailed Student's *t* test. Scale bars, 1 µm.

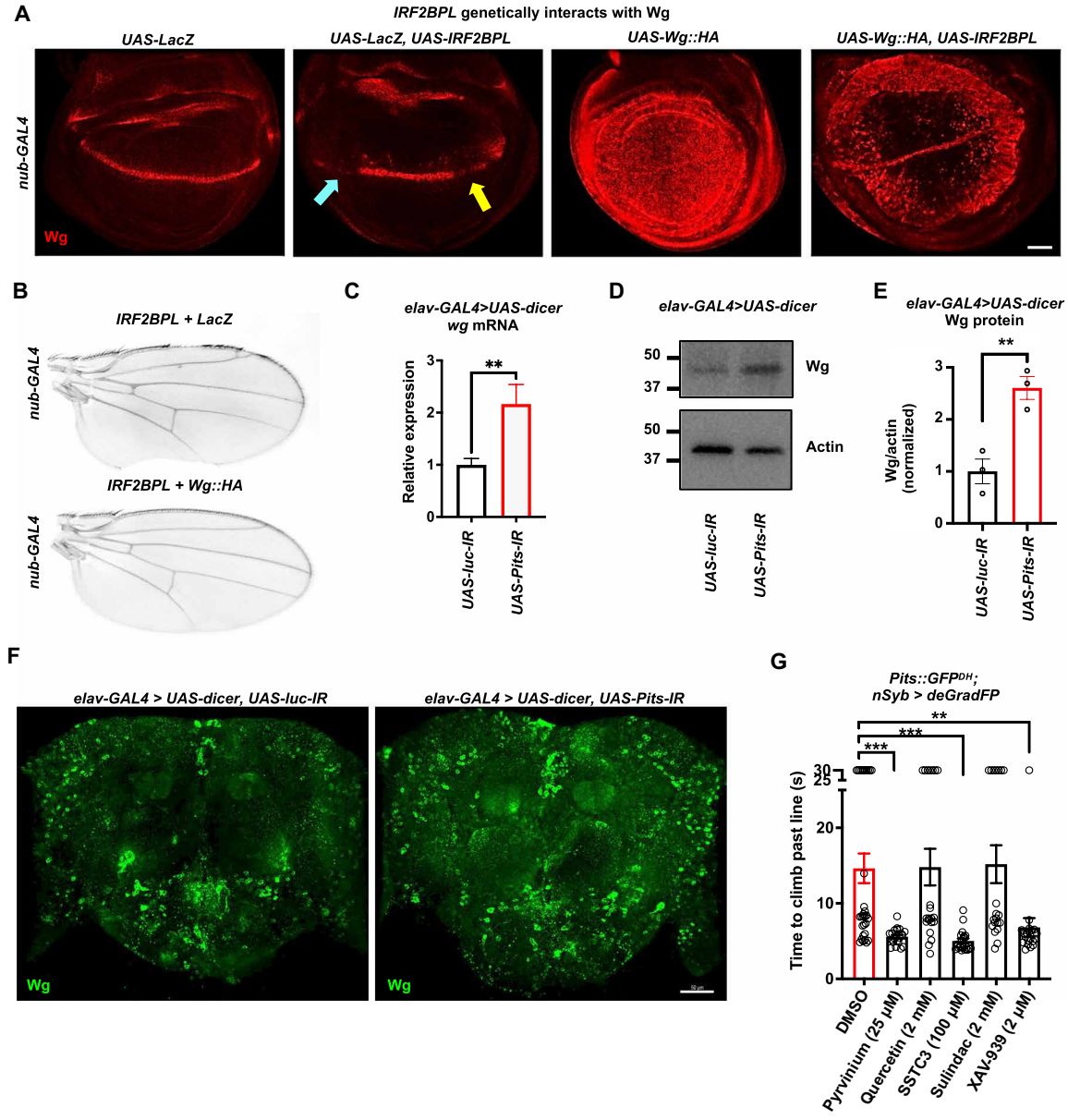

Fig. 3. Wingless genetically interacts with IRF2BPL, and neuronal reduction of Pits in neurons leads to increased *wg* transcription. (**A** and **B**) Coexpression of *UAS-IRF2BPL* with *UAS-Wg::HA*, but not *UAS-LacZ*, in the wing disc using *nub-GAL4* at 18°C restores Wg expression along the DV boundary (A) and the adult wing margin morphology (B). Scale bar, 40 μm. (**C** to **F**) Neuronal reduction of Pits via RNAi using *elav-GAL4, UAS-dicer* results in increased *wg* transcript (C) by qPCR and Wg protein (D) in 20 d.p.e. fly heads, as quantified in (E) and by immunohistochemistry (F) in the adult brain of 20-day-old flies stained for Wg. Results are means ± SEM (**$P < 0.01$). Statistical analyses were determined by two-tailed Student's *t* test. Scale bar, 50 μm. (**G**) Climbing assessment of *Pits::GFP^{DH}; nSyb-GAL4, UAS-deGradFP* flies at 25 d.p.e. after adult-specific reduction of Pits::GFP and treatment with DMSO or indicated Wnt inhibitors. Time (seconds) required for flies of the indicated genotypes to climb past 7 cm ($n > 20$ per genotype). Statistical analyses were determined by ANOVA followed by Tukey post hoc. Results are means ± SEM (**$P < 0.01$ and ***$P < 0.001$).

neuronal knockdown of *Pits* (Fig. 3F). Hence, Pits negatively regulates the levels of *wg* in the brain.

To determine whether down-regulation of the Wg pathway can ameliorate the behavioral deficits observed upon neuronal reduction of Pits, we screened multiple established Wg/Wnt inhibitors in flies. We found that multiple Wnt inhibitors, specifically pyrvinium pamoate (PubChem CID: 54680693), SSTC3 (CID: 46912682), and XAV-939 (CID: 135418940), rescued the climbing defects observed upon adult-specific Pits::GFP^{DH} reduction in fly neurons at 25 d.p.e. (Fig. 3G and table S1). These data show that inhibiting Wnt signaling is neuroprotective upon reduction of Pits.

Neuronal overexpression of *wingless* is sufficient to induce progressive neural dysfunction and axonal loss

Given that neuronal reduction of Pits leads to excess *wg* transcription in the adult central nervous system (CNS), we determined whether excess Wg ligand expression is sufficient to cause neuronal dysfunction. We expressed *UAS-Wg::HA* in neurons using *nSyb-GAL4* at

25°C. Similar to neuronal reduction of Pits, flies overexpressing *Wg* in neurons have a decreased life span and age-dependent climbing defects when compared to controls expressing *LacZ* (Fig. 4, A and B). In addition, aged *nSyb-GAL4, UAS-Wg::HA* flies displayed flight deficits (Fig. 4C). Similar defects were observed with another pan-neuronal driver, *elav-GAL4* (fig. S5, A to C). These data show that excess neuronal Wg expression results in a progressive age-dependent neural dysfunction.

To determine whether excess Wg expression is sufficient to cause peripheral axon degeneration, we examined the integrity of the wing nerve upon neuronal overexpression of *UAS-Wg::HA*. We did not observe any changes in axon number or gross morphology in the wing nerves of *nSyb-GAL4, UAS-Wg::HA* in 5-day-old flies (Fig. 4D). However, similar to neuronal reduction of Pits, aged *nSyb-GAL4, UAS-Wg::HA* flies displayed a robust decrease in axonal number and severe morphological defects at day 25 (Fig. 4E). Together, our data indicate that excess Wg expression in *Drosophila* neurons is sufficient to cause progressive behavioral deficits and axonal degeneration in vivo.

irf2bpl null zebrafish display neurobehavioral deficits that are suppressed by Wnt inhibitors

In contrast to flies, the zebrafish genome has four homologs of *Pits*: *irf2bp1*, *irf2bp2a*, *irf2bp2b*, and *irf2bpl*. However, *irf2bpl* is the most conserved ortholog to *IRF2BPL* (*28*). To determine whether Irf2bpl regulates *Wnt* in a vertebrate model, we generated a null allele of the zebrafish *irf2bpl* ortholog using CRISPR-Cas9. Sequencing confirmed that *irf2bpl* mutant zebrafish contained a 3–base pair (bp) insertion and a 2-bp deletion that shifts the translational reading frame after amino acid 8, truncating the protein at amino acid 90 (fig. S6, A and B). At 5 days postfertilization (d.p.f.), transcript levels of *irf2bpl* were about 80% lower in homozygous mutant animals compared to wild type (fig. S6C). Up to 3 months of age, the homozygous mutants (*irf2bpl*$^{-/-}$) are viable, fertile, and morphologically indistinguishable from wild-type and heterozygous siblings. However, at 5 d.p.f., we found that the *irf2bpl*$^{-/-}$ mutants displayed lower total activity during a 24-hour day and night cycle, compared to wild-type sibling controls (fig. S6D). At 7 d.p.f., using an established locomotor and dark challenge assay, we found that *irf2bpl*$^{-/-}$ mutants displayed reduced locomotor activity, as well as lower bout activity (startle response) elicited by a sudden transition from light to dark, compared to wild-type siblings (Fig. 5A). These data indicate that the *irf2bpl*$^{-/-}$ fish, while morphologically and developmentally normal, display altered neuronal function. In agreement with our results in *Drosophila*, we observed increased level of Wnt1 protein in mutant heads compared to wild-type sibling controls (Fig. 5B). Furthermore, *wnt1* transcription and the downstream Wnt-responsive gene, *lef1*, were increased in the mutant animals compared to the wild-type siblings (Fig. 5C and fig. S6E). These data show that, similar to flies, Wnt signaling is up-regulated upon loss of *irf2bpl* in zebrafish.

We next sought to determine whether Wnt inhibition could suppress the behavioral phenotypes we observed in *irf2bpl*$^{-/-}$ fish and prioritized testing drugs that were efficacious in flies (Fig. 3G). Since pyrvinium is poorly absorbed by the gut and shows poor bioavailability (*29*), we tested SSTC3 and XAV-939 in the *irf2bpl* zebrafish mutants. Treatment with either SSTC3 or XAV-939 led to a decrease in the expression of *lef1* in *irf2bpl*$^{-/-}$ mutants (Fig. 5C), indicating that these drugs can suppress the enhanced Wnt signaling in these animals. Upon treatment with SSTC3 at 4 d.p.f., *irf2bpl*$^{-/-}$ animals did not display improved locomotor function, but the response to the dark challenge significantly improved in these mutant animals compared to the dimethyl sulfoxide (DMSO)–treated group at 7 d.p.f. (Fig. 5, D and E). Similar to SSTC3, treatment with XAV-939 at 4 d.p.f. also resulted in partial phenotypic rescue of the dark challenge compared to DMSO-treated mutants at 7 d.p.f. (Fig. 5, F and G). Our data suggest that, similar to flies, the increased Wnt signaling observed upon loss of *Irf2bpl* is, at least partially, responsible for neural dysfunction in zebrafish, and pharmacological inhibition of Wnt signaling was effective at restoring some of the functional outcomes observed in these animal models.

WNT1 is increased in *IRF2BPL* patient cells

To confirm whether *WNT1* is altered in human cells, we converted NEDAMSS patient fibroblasts into induced astrocytes (*30*, *31*). Three different patient cell lines were used harboring de novo heterozygous truncations in *IRF2BPL* (table S2). Consistent with our data generated in model organisms, these cells show increased *WNT1* transcript (Fig. 6A) and protein levels (Fig. 6, B and C) when compared to three healthy controls. This indicates that NEDAMSS-associated truncations inhibit the negative regulation of WNT1 by IRF2BPL.

IRF2BPL physically and genetically interacts with CkIα

To shed insight into how Pits/IRF2BPL inhibits *Wnt* transcription, we identified interacting partners of Pits in the fly brain by performing coimmunoprecipitation followed by mass spectrometry (IP-MS) using Pits::GFP^{DH} fly heads (table S3). Intriguingly, we found a key β-catenin (Armadillo in *Drosophila*) destruction complex member, CkIα (casein kinase Iα), as one of the top binding partners of Pits (fig. S7A). We confirmed that Pits interacts with CkIα endogenously by performing co-IP of Pits::GFP^{DH} from fly heads using a human anti-CSNK1E antibody that cross-reacts with CkIα on Western blot (Fig. 7A).

CkIα is a negative regulator of Wg/Wnt signaling (*32*, *33*) but may play a role in affecting *wg* transcription, as *CkIα* RNAi in the *Drosophila* embryo causes increased *wg* transcription (*34*). In line with this, we observed that knockdown of *CkIα* in the posterior wing using *en-GAL4* leads to an increase of the *wg-lacZ* reporter gene in the posterior wing disc (fig. S7B). We therefore hypothesized that Pits/IRF2BPL acts through CkIα to inhibit Wnt transcription. To determine this, we tested whether down-regulation of CkIα by RNAi (*UAS-CkIα-IR*) can rescue the wing margin loss upon overexpression of IRF2BPL. In the adult wing, coexpression of *UAS-IRF2BPL* and *UAS-LacZ* complementary DNA (cDNA) causes wing margin loss as observed previously (>94% penetrant) (Fig. 7B). However, knockdown of *CkIα* while overexpressing IRF2BPL results in mostly normal wings (>84% normal) (Fig. 7B). Fittingly, we found that co-expression of *UAS-IRF2BPL* and *UAS-LacZ* leads to decreased Wg protein in the DV boundary, and knockdown of CkIα restores Wg protein levels (Fig. 7C) and the Wg downstream effector Cut (fig. S7C) when *IRF2BPL* is overexpressed. Together, these data indicate that IRF2BPL and CkIα genetically interact to modulate *wg* levels.

Given the in vivo physical interaction between Pits and CkIα and the genetic interaction between IRF2BPL and CkIα, we sought to determine whether promoting CkIα upon reduction of Pits protein is beneficial in neurons. Adult-specific neuronal overexpression of *UAS-CkIα::HA* ameliorates the climbing and survival defects observed upon neuronal degradation of Pits::GFP^{DH} when compared

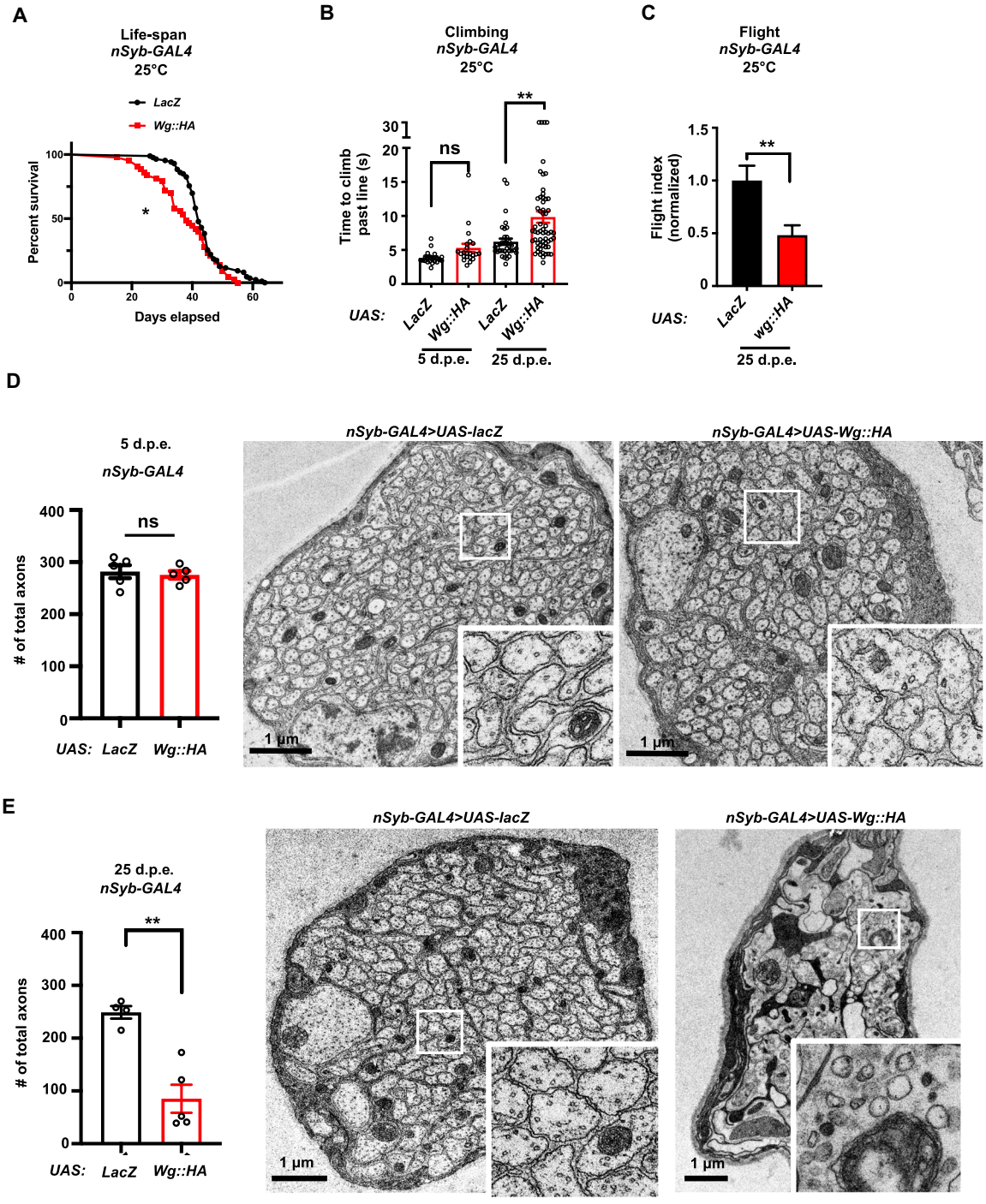

Fig. 4. Neuronal expression of Wg ligand is sufficient to cause progressive climbing defects and axonal loss. (**A**) Survival curves for neuronal expression of *UAS-LacZ* or *UAS-Wg::HA* using *nSyb-GAL4* at 25°C. A minimum of 43 flies per genotype (*$P < 0.05$). Statistical analyses were determined by the log-rank test. (**B**) *nSyb-GAL4, UAS-Wg::HA* flies exhibit progressive climbing defects. Time (seconds) required for flies of the indicated genotypes to climb past 7 cm ($n > 20$ per genotype). Statistical analyses are one-way ANOVA followed by a Tukey post hoc test. Results are means ± SEM (**$P < 0.01$). (**C**) *nSyb-GAL4, UAS-Wg::HA* flies exhibit flight defects at 25 d.p.e. compared to *nSyb-GAL4, UAS-LacZ* controls when dropped into the center of a 2-liter graduated cylinder ($n > 32$ per genotype). Results are means ± SEM (**$P < 0.01$). Statistical analyses were determined by two-tailed Student's *t* test. (**D** and **E**) Transmission electron microscopy of the peripheral wing nerves containing peripheral neurons of the anterior wing margin. Quantification shows the total axon number at (E) 5 d.p.e. upon neuronal (*nSyb-GAL4*) overexpression of *UAS-LacZ* or *UAS-Wg::HA* ($n = 5$ each genotype) and the same genotypes at 25 d.p.e. (*UAS-LacZ*, $n = 4$; *UAS-Wg::HA*, $n = 5$). Results are means ± SEM (**$P < 0.01$). Statistical analyses were determined by two-tailed Student's *t* test. Scale bars, 1 µm.

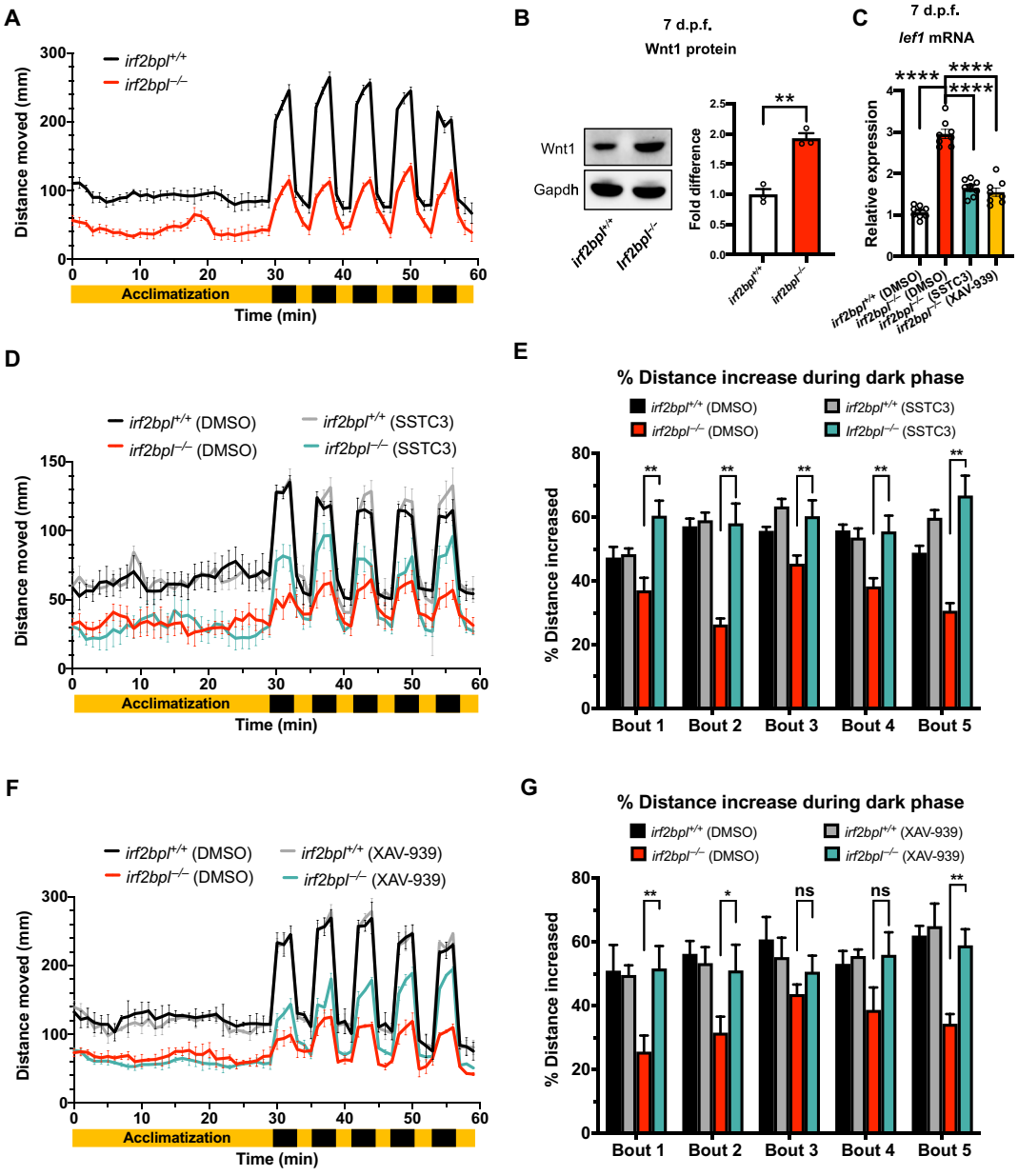

Fig. 5. Loss of irf2bpl in zebrafish leads to defective locomotor activity and increased Wnt1 signaling. (**A**) Distance moved (in millimeters) of mutants (*irf2bpl*$^{-/-}$) and wild-type sibling controls (*irf2bpl*$^{+/+}$) measured at 7 d.p.f. in a locomotor assay. During the assay, test animals were first habituated for 30 min, followed by five light-dark cycles for a total of 30 min ($n = 36$ and 47 for *irf2bpl*$^{+/+}$and *irf2bpl*$^{-/-}$ animals, respectively). (**B**) Representative Western blot and quantification of Wnt1 protein expression in *irf2bpl*$^{-/-}$ brain compared to *irf2bpl*$^{+/+}$ controls ($n = 3$ per group). (**C**) Analyses of lef1 transcript expression real-time qPCR in *irf2bpl*$^{-/-}$ treated with DMSO, SSTC3, or XAV-939, compared to *irf2bpl*$^{+/+}$ treated with DMSO ($n = 8$ per group). (**D** and **E**) Treatment with SSTC3 significantly improved the *irf2bpl*$^{-/-}$ mutants' bout activity when transitioning from a light to dark condition, compared to mutants treated with DMSO ($n = 22$ and 24 for DMSO-treated *irf2bpl*$^{+/+}$ and *irf2bpl*$^{-/-}$ animals; 25 and 23 for SSTC3-treated *irf2bpl*$^{+/+}$ and *irf2bpl*$^{-/-}$, respectively). (**F** and **G**) Similar to SSTC3, treatment with XAV-939 significantly improved the mutants' bout activity compared to DMSO-treated mutants ($n = 21$ and 19 for DMSO-treated *irf2bpl*$^{+/+}$ and *irf2bpl*$^{-/-}$ animals; 36 and 45 for XAV-939–treated *irf2bpl*$^{+/+}$ and *irf2bpl*$^{-/-}$ animals, respectively). Results are means ± SEM (*$P < 0.05$, **$P < 0.001$, and ****$P < 0.0001$).

to *UAS-LacZ* expression as a control (Fig. 7, D and E). Hence, promoting CkIα to inhibit Wg in neurons provides some protection upon reduction of Pits. To determine whether the physical interaction between IRF2BPL-CkIα (CSNK1A1) is conserved in human cells, we coimmunoprecipitated CSNK1A1 in the SH-SY5Y neuroblastoma cell line and confirmed that CSNK1A1 interacts with IRF2BPL (Fig. 7F). Hence, the Pits/IRF2BPL-CkIα interaction is conserved in humans. Last, we immunostained SH-SY5Y cells with IRF2BPL and CSNK1A1 antibodies. Not surprisingly, IRF2BPL resides predominantly in the nucleus of these cells, whereas CSNK1A1 is located throughout the cytoplasm and nucleus (Fig. 7G). However, we observed a clear colocalization of IRF2BPL and CSNK1A1 (Fig. 7G,

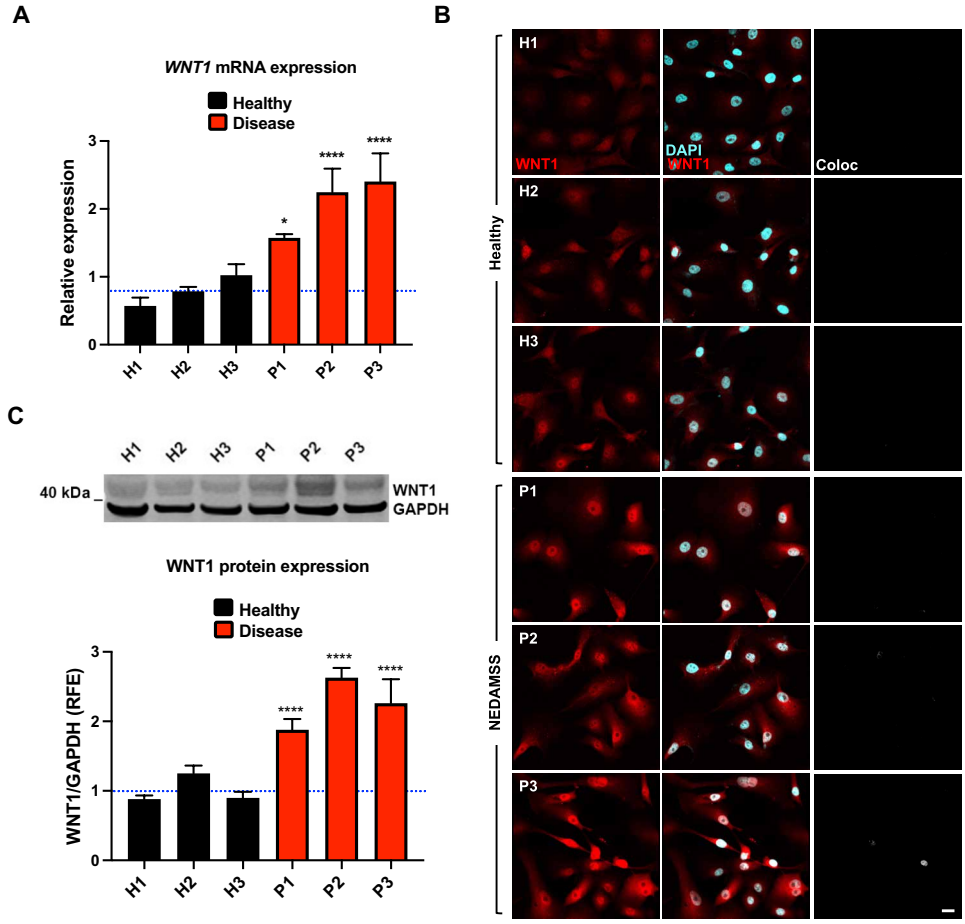

Fig. 6. Reprogrammed astrocytes from NEDAMSS patients display increased *WNT1* transcription and protein. (**A** to **C**) *WNT1* transcript (A) and protein (B and C) are elevated in reprogrammed astrocytes derived from fibroblasts of NEDAMSS patients and healthy controls by qPCR (A), immunofluorescence (B), and Western blot (C). RFE, relative fold expression. ANOVA followed by Dunnett's multiple comparison test between the mean of the controls and the mean of each line was computed to derive the *P* value: **P* < 0.05 and *****P* < 0.0001. The experiments were conducted three times. Scale bar, 20 μm.

merge in white) in the nucleus. Together, these data suggest that IRF2BPL inhibits *Wnt* transcription and downstream signaling via its interaction with CKIα in the nucleus (Fig. 7H).

DISCUSSION

Here, we explore the function of Pits/IRF2BPL in *Drosophila*, zebrafish, and human cells. We find that Pits or IRF2BPL decreases *wg* transcription in flies upon overexpression. Our data show that IRF2BPL exhibits a strong antagonistic relationship with Wg and that the IRF2BPL inhibition of Wg expression is mediated by CkIα. Loss of Pits/IRF2BPL increases *wg*/*wnt1*/*WNT1* in flies, fish, and patient cells. Reducing the level of Pits in adult neurons in flies leads to a shortened life span, progressive climbing defects, and gradual loss of peripheral axons, and these phenotypes are also associated with increased *wg* transcripts and proteins in the brain. The neurobehavioral phenotypes can be suppressed by inhibition of Wg expression by neuronal overexpression of *CkIα* or the use of drugs that inhibit Wnt signaling by increasing CkIα activity.

In contrast to flies, loss of *irf2bpl* in zebrafish does not cause lethality. However, in zebrafish, there are four irf2bp family members that likely partially compensate for *irf2bpl* loss. However, the *irf2bpl* null mutant fish display reduced locomotor activity and optomotor startle response associated with both increased *wnt1* transcript, protein, and Wnt signaling activation. The optomotor startle response requires complex neural circuitry (*35*), and the deficits in these fish could be at least partially rescued by Wnt inhibition.

To model the neuronal loss of IRF2BPL in patients, we decreased the Pits levels in adult neurons by 50 to 60%. This leads to age-dependent phenotypes in flies that are reminiscent of the progressive phenotypes observed in patients with truncations of *IRF2BPL*. Individuals with NEDAMSS often progress in development as expected for their age, and the onset of symptoms usually does not occur until the mean age of 5, with some cases only developing disease signs in adolescence (*1*, *2*, *36*–*44*). Decline in motor skills continues until patients become fully dependent of caretakers. Moreover, brain imaging studies in older patients show progressive cerebral and cerebellar atrophy, strongly suggesting severe neuronal loss (*1*) consistent with our observations in flies.

Loss of *Pits/irf2bpl/IRF2BPL* leads to excess *Wnt* transcription in multiple model systems. Reports of increased Wnt transcription and/or signaling in neurodegenerative diseases remain sparse (*45*–*47*) and controversial (*48*). In flies, mutant Huntington overexpression leads to hyperstabilization of β-catenin (*49*). In mice, it has been

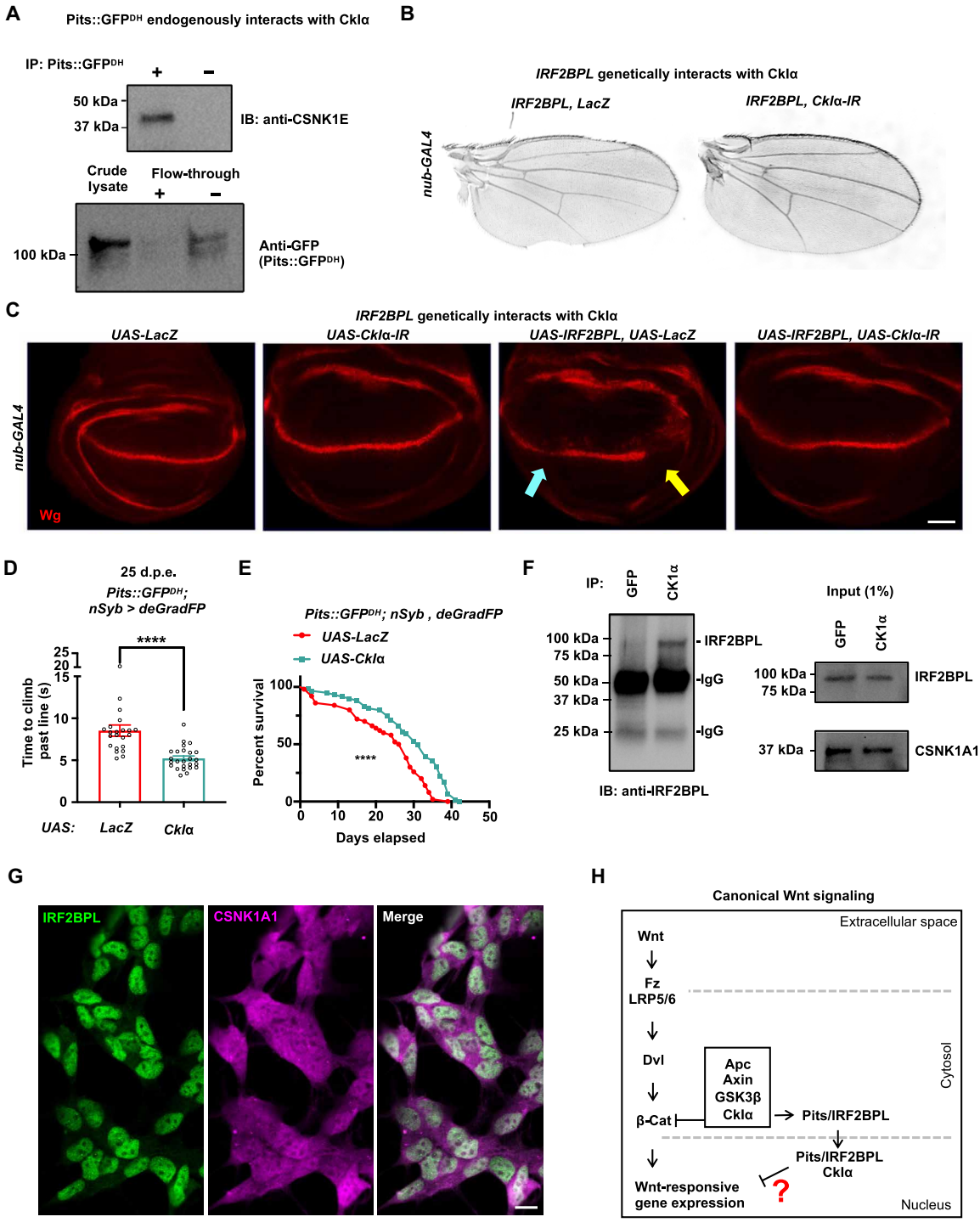

Fig. 7. Pits physically and genetically interacts with Cklα. (**A**) Pulldown of Pits::GFP^{DH} from fly heads indicates that endogenous Cklα interacts with Pits detected by Western blotting using anti-CSNK1E antibody (Cklα size is ~38 kDa). Interaction observed in triplicate. (**B** and **C**) Coexpression of *UAS-IRF2BPL* with *UAS-Cklα-IR*, but not *UAS-LacZ*, in the wing disc using nub-GAL4 at 18°C restores adult wing margin morphology (B) and Wg expression along the DV boundary (C). Scale bar, 40 μm. (**D**) *Pits::GFP^{DH}; nSyb-GAL4, UAS-deGradFP* coexpressing either *UAS-LacZ* or *UAS-Cklα::HA*. Time (seconds) required for flies of the indicated genotypes to climb past 7 cm ($n > 22$ per genotype). Statistical analyses were determined by two-tailed Student's *t* test. (**E**) Survival curves for *Pits::GFP^{DH}; nSyb-GAL4, UAS-deGradFP* coexpressing either *UAS-LacZ* or *UAS-Cklα::HA*. *n* is a minimum of 49 flies per genotype (****$P < 0.0001$). Statistical analyses were determined by the log-rank test. (**F**) In vitro coimmunoprecipitation of CKIα (CSNK1A1) or GFP as a control in SH-SY5Y cells showing an interaction with endogenous IRF2BPL. IgG, immunoglobulin G. (**G**) SH-SY5Y cells stained with IRF2BPL and CSNK1A1. Scale bar, 10 μm. (**H**) Schematic depicting the canonical Wnt pathway, highlighting potential actions of Pits/IRF2BPL.

reported that activation of Wnt signaling is a prodromal feature of a model of frontotemporal dementia with parkinsonism-17 (FTDP-17) in *tau* transgenic mice (*47*). Recently, a pediatric patient harboring a loss-of-function truncation in the negative Wnt regulator, *YPEL3*, presented with severe nervous system demyelination and axonal loss (*50*, *51*). Systems-level analysis in human cells indicates that canonical and noncanonical activation of Wnt signaling by Wnt1 alters a network of genes related to neurodegenerative diseases (*52*), and much of what is known about Wnt function in the CNS relates to neural development. For example, neuronal and glial secretion of Wg at the developing *Drosophila* neuromuscular junction regulates glutamate receptor clustering (*53*), suggesting that sustained Wnt signaling may lead to Ca^{2+} excitotoxicity (*54*). Moreover, excess Wnt signaling during neuronal differentiation results in cell cycle reentry, leading to apoptosis (*55*). We found that removal of Pits in the adult brain leads to an increase in *wg* transcription, which contributes to neuron loss. Moreover, ectopic expression of the Wg ligand alone is sufficient to cause decreased life span, progressive behavioral abnormalities, and axonal loss, phenotypes that are notably similar to a neuronal reduction of Pits. In conclusion, excess Wnt alone in neurons can lead to progressive neuronal demise. Given that Wg has been shown to refine its own expression in development (*56*), this refinement and a role for IRF2BPL may be important for long-term neuronal homeostasis.

An important question that arises from our observations is the precise subcellular location where Pits and IRF2BPL are functioning to prevent neurodegeneration. The two proteins have been characterized as DNA binding, putative E3 ligases that are predominantly found in the nucleus (*1*, *57*). Our data support a requirement for the nuclear localization of IRF2BPL, as removal of the NLS abolishes Wnt inhibition. Moreover, in SH-SY5Y cells, we found that IRF2BPL and CSNK1A1 colocalize in the nucleus. However, CkIα is mostly known for its role in the cytoplasmic Wnt destruction complex (*34*), and CkIα and its human ortholog CSNK1A1 physically interact with Pits/IRF2BPL. CkIα has also been shown to be present in the nucleus in flies and vertebrates, where it has been implicated in the DNA damage response and nuclear organization (*58*–*61*). Moreover, CkIα nuclear protein interactions have been shown to be important in modulating both Wnt activity (*62*) and the nuclear entry of transcriptional regulators (*63*) and influence *wg* transcription (*34*).

The above data suggest that increasing CkIα function upon loss of IRF2BPL observed in NEDAMSS may be protective by inhibiting excess Wnt. Two of three Wnt inhibitors that are efficacious in our models are known to function as CkIα agonists by increasing its stability (*29*). We therefore propose that IRF2BPL and CkIα interact to modulate Wnt signaling by regulating *WNT1* expression (Fig. 7H). This interaction may initiate in the cytoplasm, as a pool of Pits/IRF2BPL is present in the cytoplasm (*1*, *64*). Binding of CkIα may activate IRF2BPL and promote nuclear entry, as shown for other transcription factors (*63*). Our data indicate that, in addition to the RING domain, both DNA binding and nuclear localization are required for IRF2BPL-mediated inhibition of *Wnt* transcription. Hence, Pits/IRF2BPL, like their paralogs (IRF2BP1 and IRF2BP2), likely act as transcriptional repressors (*57*, *65*, *66*) to inhibit *Wnt* transcription, consistent with the increase in wg/*wnt1*/*WNT1* messages observed in flies, fish, and human cells. CkIα has also been documented to be in nuclear speckles where active gene regulation occurs (*59*). Hence, nuclear CkIα may also work in conjunction with IRF2BPL. An in vitro study in gastric cancer cell lines showed that IRF2BPL interacts with and targets β-catenin for proteasomal degradation (*67*). While our studies implicate that IRF2BPL downregulates Wnt transcription, its previously documented interaction with β-catenin suggests that there may be an additional role for IRF2BPL in the regulation of β-catenin function.

In summary, here, we provide compelling evidence that loss of Pits/IRF2BPL leads to excess Wnt transcription in the mature nervous system. We show that Wg ligand expression in neurons is sufficient to cause neural dysfunction and axonal loss in flies. We further identified pharmacological Wnt inhibitors that rescue neural dysfunction in flies and zebrafish. While these compounds have been generated primarily for the cancer field, repurposing them for NEDAMSS patients may be efficacious.

MATERIALS AND METHODS

Immunohistochemistry

Drosophila wing discs were dissected and imaged as previously described (*68*). Briefly, wing discs were dissected, fixed in 4% paraformaldehyde (PFA), and incubated with mouse anti-Wg (1:50) [Developmental Studies Hybridoma Bank (DSHB), 4D4], mouse anti-cut (1:50) (DSHB, 2B10), guinea pig anti-Sens (1:100) (*16*), mouse anti–β-gal (1:300) (Promega, Z3781), or rabbit anti-IRF2BPL (1:200) (Abcam, ab221099). Vectashield (Vector Labs, H-1000-10) was used for mounting. The *Drosophila* brain was stained and imaged as previously described (*1*). Adult brains were fixed immediately in 4% PFA and incubated at 4°C overnight on a shaker. Brains were postfixed with 4% PFA with 2% Triton X-100 in phosphate-buffered saline (PBST) and kept in a vacuum container for an hour to eliminate air bubbles from the tracheal tissue. After three washes with PBS with 2% PBST, brains were incubated with primary antibodies overnight at 4°C on shaker. Brains were washed 3× with 2% PBST and then incubated with secondary antibodies at room temperature for 2 hours. Samples were washed with 2% PBST (3×) and mounted on a glass slide using Vectashield (Vector Labs, H-1000-10). Primary antibodies used were mouse anti-Wg (DSHB, 4D4) 1:50 for wing disc and 1:10 for the adult brain. Secondary antibody used was anti-mouse 647 (Jackson ImmunoResearch, 715-605-151) 1:250. Both wing discs and brains were scanned using a laser confocal microscope (Zeiss LSM 880), and images were processed using ZEN (Zeiss) and Imaris (Oxford Instruments) software.

NEDAMSS patient and healthy control fibroblasts were directly reprogrammed to astrocytes using a previously published method (*30*, *31*). The reprogrammed astrocytes were seeded at 30,000 cells per 24-well plate and plated in 10% fetal bovine serum (FBS) culture medium. The next day, they were fixed and stained as previously described (*30*, *31*) with rabbit anti-WNT1 (Abcam, ab63934) 1:250 and 4′,6-diamidino-2-phenylindole (DAPI; Invitrogen, D1306) followed by anti-rabbit Alexa Fluor secondary antibody (Thermo Fisher Scientific, A32732). Images were obtained with a Zeiss 800 confocal microscope. Colocalization of WNT1 with DAPI was achieved via colocalization function in Imaris (Oxford Instruments) software.

Transmission electron microscopy

Transmission electron microscopy imaging of *Drosophila* wing margins was performed as previously described (*24*). Briefly, the fly thorax was rapidly dissected by removal of the head and abdomen, and wings were cut and fixed in 2% PFA and 2.5% glutaraldehyde in 0.1 M sodium cacodylate buffer (pH 7.2). The thorax with attached

wings was fixed on a rotator at 4°C for up to 2 days. Samples were rinsed in fixative followed by three washes with Millipore H_2O. Samples were submerged in 1% osmium tetroxide for 45 min at room temperature. Dehydration was performed by benchtop incubations of samples with 25, 50, 75, 90, and 100% ethanol (EtOH) that was followed by propylene oxide. The samples were then progressively infiltrated by increasing ratios of propylene oxide:Embed 812 resin (1:3, 1:1, and 3:1) until incubated in 100% Embed 812 resin (3×) and rotated overnight at room temperature. The samples were then embedded into flat silicone molds and cured at 62°C for 3 days. Polymerized samples were cut at 48 to 50 nm and stained with 1% uranyl acetate for 10 min followed by 2.5% lead citrate for 2 min. Grids were viewed in a JEOL 1400+ transmission electron microscope at 80 kV, and images were captured using an AMT XR-16 mid-mount 16-megapixel digital camera.

Protein isolation, electrophoresis, and Western blot

For fly, protein biochemistry was performed as previously described (*1*). Briefly, protein was isolated from fly heads, where five heads were dounced with a homogenizer (3× for 10 s on ice) in 30 μl of radioimmunoprecipitation assay buffer (Thermo Fisher Scientific, 89900) with protease inhibitor (GenDepot, P3100-001). Thirty microliters of 2× Laemmli buffer (Bio-Rad, 1610737) containing 10% β-mercaptoethanol was added to the samples and heated at 95°C for 5 min. After a 5-min spin at 14,000 rpm at 4°C, supernatants were loaded and run on 4 to 20% gradient polyacrylamide gels (Bio-Rad, Mini-PROTEAN TGX). Protein was transferred to polyvinylidene difluoride (PVDF) membranes and blocked with milk for 40 to 60 min. Primary antibodies were incubated overnight at 4°C. The following antibodies were used in the present study: mouse anti-Wg (1:100) (DSHB, 4D4), mouse anti-actin (1:20,000) (EMD-Millipore, C4), rabbit anti-GFP (1:5000) (Invitrogen, A-11122), mouse anti-CSNK1E (1:500) (DSHB, 13D7), rabbit anti-CSNK1A1 (1:1000) (Abcam, ab206652), and anti-rabbit IRF2BPL (1:1000) (Invitrogen, PA5-62256). Horseradish peroxidase–conjugated secondary antibodies available at Jackson ImmunoResearch were used to detect the respective primary antibody. Protein was detected with Western Lightning Chemiluminescence Reagent Plus (PerkinElmer, NEL104001EA) enhanced chemiluminescence (ECL) solution using the Bio-Rad ChemiDoc MP Imaging System.

For zebrafish, protein lysates were isolated from the heads of 16 zebrafish irf2bpl mutants or wild-type siblings at 7 d.p.f. Fifty microliters of 4× Laemmli buffer (Bio-Rad, 161-0747) containing 10% β-mercaptoethanol was added to the samples, which were then homogenized and heated at 95°C for 5 min. After a 5-min spin at 14,000 rpm at 4°C, supernatants were loaded and run on 4 to 20% gradient polyacrylamide gels (Bio-Rad, Mini-PROTEAN TGX). Protein was transferred to PVDF membranes and blocked with 5% milk for 30 min. Primary antibodies were incubated overnight at 4°C. The following antibodies were used in the present study: Rabbit anti-Wnt1 (Invitrogen, 36-5800) and rabbit anti-Gapdh (Cell Signaling Technology, 2118S) were used as primary antibodies. Horseradish peroxidase–conjugated anti-rabbit secondary antibodies were used to detect the respective primary antibody. Protein was detected with Pierce ECL Western blotting substrate using the Bio-Rad ChemiDoc MP Imaging System.

For reprogrammed astrocyte lysates, rabbit anti-WNT1 (1:1000; Abcam, ab63934) and mouse anti–glyceraldehyde-3-phosphate dehydrogenase (GAPDH) (1:5000; Millipore, MAB374) were used as primaries, followed by appropriate fluorescent conjugated secondaries (LI-COR). The blots were imaged by LI-COR Odyssey CLx and quantified with Image Studio Lite.

Quantitative real-time PCR

For transcript expression analyses in *Drosophila*, total RNA was isolated from 40 heads of *elav-GAL4, UAS-Dicer, UAS-Pits-IR* or *elav-GAL4, UAS-Dicer, UAS-luc-IR* at 20 d.p.e. using the RNeasy Plus Mini Kit (Qiagen). cDNA was generated using 5× All-In-One RT MasterMix (Applied Biological Materials Inc.) as per the manufacturer's protocol. Real-time quantitative polymerase chain reaction (qPCR) was performed using Fast SYBR Green Master Mix (Applied Biosystems) using the following gene-specific primers: 5′-CCAAGTCGAGGGCAAACAGAA-3′ (forward) and 5′-TGGATCGCTGGGTCCATGTA-3′ (reverse) for *wg* (Fig. 3C) and 5′-GAGGGGCAAAAATCTATTCGGC-3′ (forward) and 5′-GCTGGTGATTGCGTAAATGAAG-3′ (reverse) for *wg* (fig. S4D). Triplicate reactions for each cell line were run on an Applied Biosystems QuantStudio 6 machine. *Tub* was used as an internal control, and the fold changes of target genes were calculated using the $2^{-\Delta\Delta Cq}$ method.

For transcript expression analyses in zebrafish, total RNA was isolated from 24 embryos of irf2bpl mutants or wild-type siblings at 7 d.p.f. and converted into cDNA using the iScript cDNA Synthesis Kit (Bio-Rad) based on the manufacturer's protocol. Real-time qPCR was performed using iTaq Universal SYBR Green PCR mix (Bio-Rad) using the following gene-specific primers: 5′-GTCGTTGGAACTGTCCCACT-3′ (forward) and 5′-GTCACAGGTGCAGGACTCAA-3′ (reverse) for *wnt1*; 5′-TCCTCTGGGTTGGTTCTCAC-3′ (forward) and 5′-CTGCTCCTTTCTCTGCTCGT-3′ (reverse) for *lef1*; 5′-TGCACTCCTTTTGACGTGAG-3′ (forward) and 5′-TGCCAAAGTCTTTCATGCAG-3′ (reverse) for *irf2bpl*.

For transcript expression analyses in human cells, total RNA was extracted from differentiated human astrocytes by standard TRIzol protocols and converted to cDNA using the RevertAid First Strand cDNA Synthesis Kit (Thermo Fisher Scientific) based on the manufacturer's guidelines. Real-time qPCR was performed using Power SYBR Green master mix (Thermo Fisher Scientific) and *WNT1*-specific primer set 5′-TAAGCAGGTTCGTGGAGGAG-3′ (forward) and 5′-GGTTTCTGCTACGCTGCTG-3′ (reverse). Triplicate reactions for each cell line were run on an Applied Biosystems QuantStudio 6 machine. GAPDH was used as an internal control, and the fold changes of target genes were calculated using the $2^{-\Delta\Delta Cq}$ method.

Generation and maintenance of zebrafish irf2bpl mutant

The zebrafish *irf2bpl* mutant line was generated using CRISPR-Cas9 with single-guide RNA target sequence 5′-ACACGACTGTCTCCTCGACG-3′ made by Integrated DNA Technologies according to the manufacturer's protocol. Mutant animals were genotyped and sequenced using primers 5′-GGCTCCGTAAAATCCCAAAT-3′ and 5′-AGCAGCTCAACATGTCTTCG-3′. The *irf2bpl* heterozygous mutant containing a 3-bp insertion and a 2-bp deletion in that targeted sequence was outcrossed to the parental AB strain for at least two generations before use in experiments to eliminate potential off-target variants. After each assay described below, tested animals were individually genotyped using PCR with primers 5′-GGCTCCGTAAAATCCCAAAT-3′ and 5′-AGCAGCTCAACATGTCTTCG-3′ and high-resolution melting (HRM) analysis (fig. S6C) as previously

described (*69*). All animals were maintained in the Zebrafish Research Facility at the University of Alabama at Birmingham. All fish were maintained at 28°C and kept at a 14-hour light and 10-hour dark cycle under standard laboratory conditions (*70*). All animal studies were performed according to the guidelines by the Institutional Animal Care and Use Committee of the University of Alabama.

Animal behavioral assays

For *Drosophila* behavioral assays, climbing (negative geotaxis) assays were performed as previously described (*1*). Briefly, 24 hours before testing, flies were anesthetized with CO_2 and housed individually on standard fly food. At the time of testing, individual flies were transferred to a sterile vial lacking food and habituated for 1 min. Then, flies were tapped to the bottom of the vial and assessed for negative geotaxis, given 30 s to reach the 7-cm mark on the vial. Flight assays were also performed on individual flies. Flies were dropped into a 2-liter graduated cylinder via a funnel, and the fly landing site on the side of the vial was measured (in milliliters). To generate a flight index, all data were normalized to the mean value of the control flies. Life-span analysis was performed as previously described (*24*). Briefly, freshly eclosed flies were separated by genotype and sex and incubated at indicated temperatures. Flies were flipped into a fresh vial every 2 to 3 days, and survival was determined once a day. A minimum of 50 flies were tested in each assay. Statistical analysis was performed using log-rank (Mantel-Cox) test.

For zebrafish behavioral assays, and for all experiments, *irf2bpl*$^{+/-}$ heterozygous animals were in-crossed to generate wild-type (+/+), heterozygous (+/−), and homozygous (−/−) sibling progeny. For the 24-hour sleep-wake activity assay, zebrafish larvae at 5 d.p.f. were chosen randomly and placed individually into each well of a flat-bottom 24-well plate. The activity of each larva was tracked for 24 hours, consisting of 14 hours of light and 10 hours of dark using the DanioVision system (Noldus Information Technology). The average swimming distance was measured for 24 hours per 1-hour time bins using EthoVision XT software (Noldus). For the locomotor assay, larvae at 7 d.p.f. were first habituated with light-on condition in a 96-well plate for 30 min, followed by five light-dark cycles for a total of 30 min (each cycle contains 3 min of light phase and 3 min of dark phase). The swimming activity of each larva was recorded using the DanioVision system (Noldus Information Technology), and the average swimming distance and velocity were measured for 1 hour per minute bins using EthoVision XT software (Noldus). After assay, each larva was processed for DNA extraction and genotyped using PCR and HRM analyses.

Pharmacological inhibition and rescue assay

For Wnt inhibition in flies, DMSO or indicated compounds were added to the molten fly food of the parental cross at 12.5 μl/5 ml of fly food to achieve the desired final concentrations. Upon eclosure, F_1 experimental flies were placed in fresh vials with the same drug and fresh vials were provided every 2 to 3 days throughout aging. For zebrafish studies, the homozygous and heterozygous *irf2bpl* mutants and wild-type siblings were generated from in-crossing of heterozygous mutants. Embryos were treated with drugs (10 μM XAV-939 or 1 μM SSTC3) or DMSO from 4 to 7 d.p.f. The fish water and chemicals were changed once a day until assays. At 7 d.p.f., all embryos are subjected to the locomotor assay described above. All embryos were genotyped after the assay.

Table 1. List of fly stocks used in study.

Name	Genotype	Source
nSyb-GAL4	*y1 w*;; P{nSyb-GAL4.S}3*	BDSC_51635
UAS-deGradFP	w[*]; P{w[+mC]=UAS-Nslmb-vhhGFP4}3	BDSC_38421
Elav-GAL4	P{w[+mW.hs]=GawB} elav[C155]	BDSC_458
UAS-Pits	*y1 w*; PBac{UAS-Pits-RC}VK00037*	(*1*)
UAS-IRF2BPL	*y1 w*; Pbac{UAS-hIRF2BPL.B}VK00037*	BDSC_78509
UAS-LacZ	*w*; P{w[+mC]=UAS-lacZ.Exel}2*	BDSC_8529
nub-GAL4	*w* (P{GawB} nubbin-AC-62)*	BDSC_51635
UAS-IRF2BPL$^{\Delta RING}$	*y1 w*; Pbac{UAS-hIRF2BPL.ΔRING} VK00037*	This study
UAS-IRF2BPL$^{\Delta DNA-BD}$	*y1 w*; Pbac{UAS-hIRF2BPL.ΔDNA-BD} VK00037*	This study
UAS-IRF2BPL$^{\Delta NLS}$	*y1 w*; Pbac{UAS-hIRF2BPL.ΔNLS} VK00037*	This study
UAS-Wg::HA	*w*; P{w[+mC]=UAS-wg.H.T:HA1}6C*	BDSC_5918
Act-GAL4	*y1 w*; P{w+mC = Act5C-GAL4}25FO1/ CyO, y+*	BDSC_4414
UAS-Pits$^{\Delta RING}$	*y1 w*; Pbac{UAS-Pits-RC.ΔRING}VK00037*	This study
UAS-Pits$^{\Delta DNA-BD}$	*y1 w*; Pbac{UAS-Pits-RC.ΔDNA-BD}VK00037*	This study
UAS-IRF2BPL^{RING}	*y1 w*; Pbac{UAS-hIRF2BPL.RING} VK00037*	This study
UAS-IRF2BPL^{DNA-BD}	*y1 w*; Pbac{UAS-hIRF2BPL.DNA-BD} VK00037*	This study
en-Gal4, NRE-GFP, UAS-RFP	en-Gal4, UAS-myr::mRFP, NRE-GFP	BDSC_30729
elav-GAL4, UAS-dicer	P{w[+mW.hs]=GawB} elav[C155] w[1118]; P{w[+mC]=UAS-Dcr-2.D}2	BDSC_25750
Pits 20-kb GR	*y1 w*; Pbac{CH322-141N09}VK00037*	(*1*)
UAS-Cklalpha-IR	*y1 v1; P{TriP.JF01792} attP2*	BDSC_25786
UAS-Cklalpha::HA	*w*; P{UAS-Cklα.HA}1/ CyO*	BDSC_55067
UAS-Dsh	*w*; P{UAS-dsh.myc}1-16*	BDSC_9453
wg-lacZ	*P{PZ}wg02657 cn1/ CyO; ry506*	BDSC_11205

Adult wing imaging and analysis

Drosophila wings were mounted and imaged as previously described (*68*). Briefly, adult wings were dissected in 70% EtOH and mounted in a 3:1 dilution of CMCP-10 mounting medium (Masters, Wood Dale, IL) and lactic acid for imaging. Images were obtained with a Leica MZ16 stereomicroscope equipped with an Optronics MicroFire camera and Image-Pro Plus 7.0. For Dsh-IRF2BPL interaction analysis in the adult wing, the number of single large blisters (visible without microscope), as well as the total number of smaller blisters, was counted. The ectopic bristles between the L1 and L2 wing veins were manually counted and compared across genotypes at the indicated temperature.

Fibroblast reprogramming to astrocyte-like cells

Direct conversion of healthy and NEDAMSS patient fibroblasts was performed as previously described (*30*, *71*). NEDAMSS patients harbored truncating mutations as follows: P1, p.Y173X; P2, p.R188X; P3, p.A708fs*59. Briefly, fibroblasts were treated with retroviral vectors OCT3, SOX2, KLF4, and c-MYC in fibroblast culture medium. After 48 hours, the medium was changed to NPC conversion medium [Dulbecco's modified Eagle's medium (DMEM)/F12, 1% N2, 1% B27, epidermal growth factor (40 ng/ml), and fibroblast growth factor (20 ng/ml)]. Attached cells that proliferated were split upon 100% confluence and collected or lifted using Accutase (StemPro Accutase Cell Dissociation Reagent, Gibco). Cells were plated onto dishes containing fibronectin (5 μg/ml; Millipore) over a period of 18 to 21 days. Small volumes of these pure iNPC cells were seeded in astrocyte medium (DMEM/GlutaMAX, 10% FBS, and 1% N2) and were further differentiated into astrocytes in 5 days.

Ethics

Human dermal fibroblasts were obtained at the University of California, Los Angeles with consent under IRB#11-001087.

Coimmunoprecipitation studies

Co-IP studies in flies were performed as previously described (*68*). Briefly, total protein was isolated from snap-frozen adult heads from *Pits::GFP*^{DH} flies homogenized in NETN buffer [100 mM NaCl, 20 mM tris-Cl (pH 8.0), and 0.5 mM EDTA] with protease inhibitor (GenDepot, P3100-001). Then, 30 μl of GFP nano-antibody agarose beads (catalog no. ABP-NAB-GFPA100) was incubated with the protein lysate in an end-over-end rotator overnight at 4°C. Agarose beads without any antibody were used as the negative control. After the overnight incubation, the agarose beads were spun at 3000 rpm for 5 min at 4°C. Supernatant was collected in a separate tube as the flow-through to check the efficiency of the IP. Subsequently, the beads were washed with NETN buffer with protease inhibitor three times followed by centrifugation at 3000 rpm at 4°C for 5 min. The elution was carried out in 10 μl of 4× Lamellae buffer. Last, the samples were boiled at 95°C and centrifuged briefly. The supernatant was used for Western blot analyses using anti-CSNK1E antibody (1:500).

Fly stocks used

Fly stocks were obtained from the Bloomington Drosophila Resource Center, generated previously or in this study. Table 1 lists the stocks used.

For IRF2BPL and Pits constructs generated in this study, the Gateway compatible entry clone for IRF2BPL (GenBank, NM_024496.3) and Pits-RC (RE41430, RC isoform) generated previously (*1*) were mutagenized with the Q5 Mutagenesis Kit (NEB, E0554S) using the primers listed in Table 2.

IP-MS analyses

Following procedures previously described (*72*), adult fly heads of *Pits::GFP*^{DH} flies were lysed in 3 volumes of NETN buffer [50 mM tris (pH 7.3), 170 mM NaCl, 1 mM EDTA, and 0.5% NP-40] using a bead beater. The lysate was removed after centrifugation at 12,000*g* for 5 min and then ultracentrifuged at 200,000*g* for 20 min at 4°C. The lysate was incubated in 20 μl of protein A Sepharose slurry (GE Healthcare Life Sciences, 17-0780-01) for 1 hour to reduce the nonspecific binding. After preclearing, the lysate was incubated with GFP-Trap beads (ChromoTek GFP-Trap) for 1 hour at 4°C. The beads were briefly washed with lysis buffer, boiled in 2× NuPAGE LDS sample buffer (Invitrogen), and subjected to

Table 2. List of primers used for site-directed mutagenesis.

Name	Strand	Primer (5′ to 3′)
IRF2BPL_DNA_BD	For	TAGGACCCAGCTTTCTTGTACAAAGTTGGC
	Rev	GCCGTGCGCCCGCTTCAG
IRF2BPL_RING_DOMAIN	For	GACCAAGTGCACCCCCAA
	Rev	CATGGTGAAGCCTGCTTTTTTG
IRF2BPL_ΔDNA_BD	For	GTCGGGGTCAAGACAGTG
	Rev	CGACATGGTGAAGCCTGC
IRF2BPL_ΔRING	For	TAGGACCCAGCTTTCTTGTACAAAG
	Rev	GAGGGGTCCGCTGTTGGC
Pits_ΔDNA_BD	For	CATGAGAACGGCGAAGTG
	Rev	CATGGTGAAGCCTGCTTTT
Pits_ΔRING	For	TAGGACCCAGCTTTCTTGTACAAAG
	Rev	CGTGGCATTCTGGGCAGC
IRF2BPL_ΔNLS	For	GGCCTCTCCGGAGCCCCC
	Rev	GCGCAGGCTGGCGGCTGCGCCCCG

SDS–polyacrylamide gel electrophoresis (NuPAGE 10% Bis-Tris Gel, Invitrogen). The eluted proteins were visualized with Coomassie Brilliant blue stain and excised into gel pieces according to the molecular weight. The individual gel piece was destained and subjected to in-gel digestion using trypsin (GenDepot, T9600). The tryptic peptides were resuspended in 10 µl of loading solution (5% methanol containing 0.1% formic acid) and subjected to nanoflow liquid chromatography–tandem MS (MS/MS) analysis with a nano-LC 1000 system (Thermo Fisher Scientific) coupled to an Orbitrap Fusion Tribrid (Thermo Fisher Scientific) mass spectrometer. The peptides were loaded onto a Reprosil-Pur Basic C18 (1.9 µm, Dr. Maisch GmbH) precolumn of 2 cm by 100 µm size. The precolumn was switched in-line with an in-house 5 cm–by–150 µm analytical column packed with Reprosil-Pur Basic C18 equilibrated in 0.1% formic acid/water. The peptides were eluted using a 35-min discontinuous gradient of 4 to 26% acetonitrile/0.1% formic acid at a flow rate of 800 nl min^{-1}. The eluted peptides were directly electrosprayed into an Orbitrap Fusion mass spectrometer. The instrument was operated in the data-dependent mode, acquiring fragmentation under direct control of the Xcalibur software (Thermo Fisher Scientific). A precursor MS spectrum was scanned at 375 to 1300 mass/charge ratio (m/z) with 120,000 resolution at 400 m/z and 5×10^5 automatic gain control (AGC) target (50 ms of maximum injection time) by the Orbitrap. Then, the top 35 strongest ions were fragmented by collision-induced dissociation with 35 normalized collision energy and 1.6 m/z isolation width and detected by Iontrap with 30 s of dynamic exclusion time, 1×10^4 AGC target, and 100 ms of maximum injection time.

Database search and data quantification for MS

The obtained MS/MS spectra were searched against target decoy Drosophila Flybase in Proteome Discoverer 1.4 interface (Thermo Fisher Scientific) with Mascot algorithm (Mascot 2.4, Matrix Science). The precursor mass tolerance was confined within 20 parts per million, with a fragment mass tolerance of 0.5 Da and a maximum of two missed cleavage sites allowed. Dynamic modification of methionine oxidation, protein N-terminal acetylation, destreak on cysteine, and ubiquitination on lysine were allowed. The peptides identified from the Mascot result file were validated using a 5% false discovery rate.

Quantification and statistical analysis

Results are presented as dot or bar plots, in which means ± SEM are depicted. All statistical analysis was performed using GraphPad Prism (GraphPad Software Inc., CA, USA). When the means of two groups were compared, a two-tailed unpaired t test was used. When more than two groups were analyzed, analysis of variance (ANOVA) was used with appropriate post hoc test described in the figure legend. Log-rank (Mantel-Cox) test was used for fly survival comparisons. Results were designated significant when $P < 0.05$: $^*P < 0.05$, $^{**}P < 0.01$, $^{***}P < 0.001$, and $^{****}P < 0.0001$; ns indicates nonsignificant.

SUPPLEMENTARY MATERIALS

Supplementary material for this article is available at https://science.org/doi/10.1126/sciadv.abl5613

View/request a protocol for this paper from *Bio-protocol*.

REFERENCES AND NOTES

1. P. C. Marcogliese, V. Shashi, R. C. Spillmann, N. Stong, J. A. Rosenfeld, M. K. Koenig, J. A. Martínez-Agosto, M. Herzog, A. H. Chen, P. I. Dickson, H. J. Lin, M. U. Vera, N. Salamon, J. M. Graham Jr., D. Ortiz, E. Infante, W. Steyaert, B. Dermaut, B. Poppe, H.-L. Chung, Z. Zuo, P.-T. Lee, O. Kanca, F. Xia, Y. Yang, E. C. Smith, J. Jasien, S. Kansagra, G. Spiridigliozzi, M. El-Dairi, R. Lark, K. Riley, D. D. Koeberl, K. Golden-Grant; Program for Undiagnosed Diseases (UD-Pr OZA); Undiagnosed Diseases Network, S. Yamamoto, M. F. Wangler, G. Mirzaa, D. Hemelsoet, B. Lee, S. F. Nelson, D. B. Goldstein, H. J. Bellen, L. D. M. Pena, IRF2BPL is associated with neurological phenotypes. *Am. J. Hum. Genet.* **103**, 245–260 (2018).
2. F. T. Mau-Them, L. Guibaud, L. Duplomb, B. Keren, K. Lindstrom, I. Marey, F. Mochel, M. J. van den Boogaard, R. Oegema, C. Nava, A. Masurel, T. Jouan, F. E. Jansen, M. Au, A. H. Chen, M. Cho, Y. Duffourd, E. Lozier, F. Konovalov, A. Sharkov, S. Korostelev, B. Urteaga, P. Dickson, M. Vera, J. A. Martínez-Agosto, A. Begemann, M. Zweier, T. Schmitt-Mechelke, A. Rauch, C. Philippe, K. van Gassen, S. Nelson, J. M. Graham Jr., J. Friedman, L. Faivre, H. J. Lin, C. Thauvin-Robinet, A. Vitobello, De novo truncating variants in the intronless IRF2BPL are responsible for developmental epileptic encephalopathy. *Genet. Med.* **21**, 1008–1014 (2019).
3. A. Rampazzo, F. Pivotto, G. Occhi, N. Tiso, S. Bortoluzzi, L. Rowen, L. Hood, A. Nava, G. A. Danieli, Characterization of C14orf4, a novel intronless human gene containing a polyglutamine repeat, mapped to the ARVD1 critical region. *Biochem. Biophys. Res. Commun.* **278**, 766–774 (2000).
4. G.-J. Liaw, Pits, a protein interacting with Ttk69 and Sin3A, has links to histone deacetylation. *Sci. Rep.* **6**, 33388 (2016).
5. Z. Steinhart, S. Angers, Wnt signaling in development and tissue homeostasis. *Development* **145**, dev146589 (2018).
6. A. Wodarz, R. Nusse, Mechanisms of WNT signaling in development. *Cell Dev. Biol.* **14**, 59–88 (1998).
7. K. M. Cadigan, M. Peifer, Wnt signaling from development to disease: Insights from model systems. *Cold Spring Harb. Perspect. Biol.* **1**, a002881 (2009).
8. R. Nusse, H. Clevers, Wnt/β-catenin signaling, disease, and emerging therapeutic modalities. *Cell* **169**, 985–999 (2017).
9. G. V. D. Ferrari, R. T. Moon, The ups and downs of Wnt signaling in prevalent neurological disorders. *Oncogene* **25**, 7545–7553 (2006).
10. N. C. Inestrosa, E. Arenas, Emerging roles of Wnts in the adult nervous system. *Nat. Rev. Neurosci.* **11**, 77–86 (2010).
11. C. A. Oliva, J. Y. Vargas, N. C. Inestrosa, Wnts in adult brain: From synaptic plasticity to cognitive deficiencies. *Front. Cell. Neurosci.* **7**, 224 (2013).
12. F. McLeod, P. C. Salinas, Wnt proteins as modulators of synaptic plasticity. *Curr. Opin. Neurobiol.* **53**, 90–95 (2018).
13. P. C. Marcogliese, S. L. Deal, J. Andrews, J. M. Harnish, V. H. Bhavana, H. K. Graves, S. Jangam, X. Luo, N. Liu, D. Bei, Y.-H. Chao, B. Hull, P.-T. Lee, H. Pan, C. M. Longley, H.-T. Chao, H. Chung, N. A. Haelterman, O. Kanca, S. N. Manivannan, L. Z. Rossetti, A. Gerard, E. M. C. Schwaibold, R. Guerrini, A. Vetro, E. England, C. N. Murali, T. S. Barakat, M. F. van Dooren, M. Wilke, M. van Slegtenhorst, G. Lesca, I. Sabatier, N. Chatron, C. A. Brownstein, J. A. Madden, P. B. Agrawal, R. Keller, L. Pavinato, A. Brusco, J. A. Rosenfeld, R. Marom, M. F. Wangler, S. Yamamoto, *Drosophila* functional screening of de novo variants in autism uncovers deleterious variants and facilitates discovery of rare neurodevelopmental diseases. bioRxiv 2020.12.30.424813 [Preprint]. 1 January 2021. https://doi.org/10.1101/2020.12.30.424813.
14. J. P. Couso, S. A. Bishop, A. M. Arias, The wingless signalling pathway and the patterning of the wing margin in Drosophila. *Dev. Camb. Engl.* **120**, 621–636 (1994).
15. C. A. Micchelli, E. J. Rulifson, S. S. Blair, The function and regulation of cut expression on the wing margin of Drosophila: Notch, Wingless and a dominant negative role for Delta and Serrate. *Development* **124**, 1485–1495 (1997).
16. R. Nolo, L. A. Abbott, H. J. Bellen, Senseless, a Zn finger transcription factor, is necessary and sufficient for sensory organ development in Drosophila. *Cell* **102**, 349–362 (2000).
17. D. Li-Kroeger, O. Kanca, P.-T. Lee, S. Cowan, M. T. Lee, M. Jaiswal, J. L. Salazar, Y. He, Z. Zuo, H. J. Bellen, An expanded toolkit for gene tagging based on MiMIC and scarless CRISPR tagging in Drosophila. *eLife* **7**, e38709 (2018).
18. E. Caussinus, O. Kanca, M. Affolter, Fluorescent fusion protein knockout mediated by anti-GFP nanobody. *Nat. Struct. Mol. Biol.* **19**, 117–121 (2012).
19. S. Nagarkar-Jaiswal, P.-T. Lee, M. E. Campbell, K. Chen, S. Anguiano-Zarate, M. C. Gutierrez, T. Busby, W.-W. Lin, Y. He, K. L. Schulze, B. W. Booth, M. Evans-Holm, K. J. T. Venken, R. W. Levis, A. C. Spradling, R. A. Hoskins, H. J. Bellen, A library of MiMICs allows tagging of genes and reversible, spatial and temporal knockdown of proteins in Drosophila. *eLife* **4**, 2743 (2015).
20. P.-T. Lee, G. Lin, W.-W. Lin, F. Diao, B. H. White, H. J. Bellen, A kinase-dependent feedforward loop affects CREBB stability and long term memory formation. *eLife* **7**, e33007 (2018).
21. K. J. T. Venken, E. Popodi, S. L. Holtzman, K. L. Schulze, S. Park, J. W. Carlson, R. A. Hoskins, H. J. Bellen, T. C. Kaufman, A molecularly defined duplication set for the X chromosome of drosophila melanogaster. *Genetics* **186**, 1111–1125 (2010).
22. K. J. T. Venken, Y. He, R. A. Hoskins, H. J. Bellen, P[acman]: A BAC transgenic platform for targeted insertion of large DNA fragments in D. melanogaster. *Science* **314**, 1747–1751 (2006).

23. J.-M. Hsu, Y. Kang, M. M. Corty, D. Mathieson, O. M. Peters, M. R. Freeman, Injury-induced inhibition of bystander neurons requires dSarm and signaling from glia. *Neuron* **109**, 473–487.e5 (2021).
24. H.-L. Chung, M. F. Wangler, P. C. Marcogliese, J. Jo, T. A. Ravenscroft, Z. Zuo, L. Duraine, S. Sadeghzadeh, D. Li-Kroeger, R. E. Schmidt, A. Pestronk, J. A. Rosenfeld, L. Burrage, M. J. Herndon, S. Chen; Members of Undiagnosed Diseases Network; Amelle Shillington, A. Shillington, M. Vawter-Lee, R. Hopkin, J. Rodriguez-Smith, M. Henrickson, B. Lee, A. B. Moser, R. O. Jones, P. Watkins, T. Yoo, S. Mar, M. Choi, R. C. Bucelli, S. Yamamoto, H. K. Lee, C. E. Prada, J.-H. Chae, T. P. Vogel, H. J. Bellen, Loss- or gain-of-function mutations in ACOX1 cause axonal loss via different mechanisms. *Neuron* **106**, 589–606.e6 (2020).
25. R. Hays, G. B. Gibori, A. Bejsovec, Wingless signaling generates pattern through two distinct mechanisms. *Dev. Camb. Engl.* **124**, 3727–3736 (1997).
26. M. Sharma, I. Castro-Piedras, G. E. Simmons, K. Pruitt, Dishevelled: A masterful conductor of complex Wnt signals. *Cell. Signal.* **47**, 52–64 (2018).
27. S. A. Purro, S. Galli, P. C. Salinas, Dysfunction of Wnt signaling and synaptic disassembly in neurodegenerative diseases. *J. Mol. Cell Biol.* **6**, 75–80 (2014).
28. Y. Hu, I. Flockhart, A. Vinayagam, C. Bergwitz, B. Berger, N. Perrimon, S. E. Mohr, An integrative approach to ortholog prediction for disease-focused and other functional studies. *BMC Bioinformatics* **12**, 357 (2011).
29. S. Jiang, M. Zhang, J. Sun, X. Yang, Casein kinase 1α: Biological mechanisms and theranostic potential. *Cell Commun. Signal* **16**, 23 (2018).
30. K. Meyer, L. Ferraiuolo, C. J. Miranda, S. Likhite, S. McElroy, S. Renusch, D. Ditsworth, C. Lagier-Tourenne, R. A. Smith, J. Ravits, A. H. Burghes, P. J. Shaw, D. W. Cleveland, S. J. Kolb, B. K. Kaspar, Direct conversion of patient fibroblasts demonstrates non-cell autonomous toxicity of astrocytes to motor neurons in familial and sporadic ALS. *Proc. Natl. Acad. Sci. U.S.A.* **111**, 829–832 (2014).
31. N. Gatto, C. D. S. Souza, A. C. Shaw, S. M. Bell, M. A. Myszczynska, S. Powers, K. Meyer, L. M. Castelli, E. Karyka, H. Mortiboys, M. Azzouz, G. M. Hautbergue, N. M. Márkus, P. J. Shaw, L. Ferraiuolo, Directly converted astrocytes retain the ageing features of the donor fibroblasts and elucidate the astrocytic contribution to human CNS health and disease. *Aging Cell* **20**, e13281 (2021).
32. S. Yanagawa, Y. Matsuda, J. Lee, H. Matsubayashi, S. Sese, T. Kadowaki, A. Ishimoto, Casein kinase I phosphorylates the Armadillo protein and induces its degradation in Drosophila. *EMBO J.* **21**, 1733–1742 (2002).
33. K. Legent, J. Steinhauer, M. Richard, J. E. Treisman, A screen for X-linked mutations affecting Drosophila photoreceptor differentiation identifies casein kinase 1α as an essential negative regulator of wingless signaling. *Genetics* **190**, 601–616 (2012).
34. C. Liu, Y. Li, M. Semenov, C. Han, G.-H. Baeg, Y. Tan, Z. Zhang, X. Lin, X. He, Control of β-catenin phosphorylation/degradation by a dual-kinase mechanism. *Cell* **108**, 837–847 (2002).
35. E. L. Troconis, A. J. Ordoobadi, T. F. Sommers, R. Aziz-Bose, A. R. Carter, J. G. Trapani, Intensity-dependent timing and precision of startle response latency in larval zebrafish. *J. Physiol.* **595**, 265–282 (2017).
36. C. Ganos, S. Zittel, U. Hidding, C. Funke, S. Biskup, K. P. Bhatia, IRF2BPL mutations cause autosomal dominant dystonia with anarthria, slow saccades and seizures. *Parkinsonism Relat. Disord.* **68**, 57–59 (2019).
37. E. Shelkowitz, J. K. Singh, A. Larson, E. R. Elias, IRF2BPL gene mutation: Expanding on neurologic phenotypes. *Am. J. Med. Genet. A* **179**, 2263–2271 (2019).
38. M. Skorvanek, P. Dusek, M. Rydzanicz, A. Walczak, J. Kosinska, G. Kostrzewa, M. Brzozowska, V. Han, P. Dosekova, Z. Gdovinova, Z. Lehotska, P. Lisowski, R. Ploski, Neurodevelopmental disorder associated with IRF2BPL gene mutation: Expanding the phenotype? *Parkinsonism Relat. Disord.* **62**, 239–241 (2019).
39. C. Spagnoli, S. Rizzi, G. G. Salerno, D. Frattini, C. Fusco, IRF2BPL gene variants: One new case. *Am. J. Med. Genet. A* **182**, 255–256 (2020).
40. M. Ginevrino, R. Battini, S. Nuovo, A. Simonati, A. Micalizzi, I. Contaldo, V. Serpieri, E. M. Valente, A novel IRF2BPL truncating variant is associated with endolysosomal storage. *Mol. Biol. Rep.* **47**, 711–714 (2020).
41. L. Prilop, R. Buchert, S. Woerz, C. Gerloff, T. B. Haack, S. Zittel, IRF2BPL mutation causes nigrostriatal degeneration presenting with dystonia, spasticity and keratoconus. *Parkinsonism Relat. Disord.* **79**, 141–143 (2020).
42. X. Qian, X. Liu, Z. Zhu, S. Wang, X. Song, G. Chen, J. Wu, H. Tang, L. Cao, Neurodevelopmental disorder caused by a truncating de novo variant of IRF2BPL. *Seizure* **84**, 47–52 (2021).
43. K. M. Johannesen, N. Nikanorova, D. Marjanovic, A. Pavbro, L. H. G. Larsen, G. Rubboli, R. S. Møller, Utility of genetic testing for therapeutic decision-making in adults with epilepsy. *Epilepsia* **61**, 1234–1239 (2020).
44. S.-Y. Hong, J.-J. Yang, S.-Y. Li, I.-C. Lee, A wide spectrum of genetic disorders causing severe childhood epilepsy in Taiwan: A case series of ultrarare genetic cause and novel mutation analysis in a pilot study. *J. Pers. Med.* **10**, 281 (2020).
45. N. Rawal, O. Corti, P. Sacchetti, H. Ardilla-Osorio, B. Sehat, A. Brice, E. Arenas, Parkin protects dopaminergic neurons from excessive Wnt/β-catenin signaling. *Biochem. Biophys. Res. Commun.* **388**, 473–478 (2009).
46. C. Smith-Geater, S. J. Hernandez, R. G. Lim, M. Adam, J. Wu, J. T. Stocksdale, B. T. Wassie, M. P. Gold, K. Q. Wang, R. Miramontes, L. Kopan, I. Orellana, S. Joy, P. J. Kemp, N. D. Allen, E. Fraenkel, L. M. Thompson, Aberrant development corrected in adult-onset Huntington's disease iPSC-derived neuronal cultures via WNT signaling modulation. *Stem Cell Rep.* **14**, 406–419 (2020).
47. M. Wiedau-Pazos, E. Wong, E. Solomon, M. Alarcon, D. H. Geschwind, Wnt-pathway activation during the early stage of neurodegeneration in FTDP-17 mice. *Neurobiol. Aging* **30**, 14–21 (2009).
48. R. A. C. M. Boonen, P. van Tijn, D. Zivkovic, Wnt signaling in Alzheimer's disease: Up or down, that is the question. *Ageing Res. Rev.* **8**, 71–82 (2009).
49. J. D. Godin, G. Poizat, M. A. Hickey, F. Maschat, S. Humbert, Mutant huntingtin-impaired degradation of β-catenin causes neurotoxicity in Huntington's disease. *EMBO J.* **29**, 2433–2445 (2010).
50. B. Blanco-Sánchez, A. Clément, S. J. Stednitz, J. Kyle, J. L. Peirce, M. McFadden, J. Wegner, J. B. Phillips, E. Macnamara, Y. Huang, D. R. Adams, C. Toro, W. A. Gahl, M. C. V. Malicdan, C. J. Tifft, E. M. Zink, K. J. Bloodsworth, K. G. Stratton, U. D. Network, D. M. Koeller, T. O. Metz, P. Washbourne, M. Westerfield, yippee like 3 (ypel3) is a novel gene required for myelinating and perineurial glia development. *PLOS Genet.* **16**, e1008841 (2020).
51. J. Zhang, X. Wen, X.-Y. Ren, Y.-Q. Li, X.-R. Tang, Y.-Q. Wang, Q.-M. He, X.-J. Yang, Y. Sun, N. Liu, J. Ma, YPEL3 suppresses epithelial–mesenchymal transition and metastasis of nasopharyngeal carcinoma cells through the Wnt/β-catenin signaling pathway. *J. Exp. Clin. Cancer Res.* **35**, 109 (2016).
52. E. M. Wexler, E. Rosen, D. Lu, G. E. Osborn, E. Martin, H. Raybould, D. H. Geschwind, Genome-wide analysis of a Wnt1-regulated transcriptional network implicates neurodegenerative pathways. *Sci. Signal.* **4**, ra65 (2011).
53. K. S. Kerr, Y. Fuentes-Medel, C. Brewer, R. Barria, J. Ashley, K. C. Abruzzi, A. Sheehan, O. E. Tasdemir-Yilmaz, M. R. Freeman, V. Budnik, Glial Wingless/Wnt regulates glutamate receptor clustering and synaptic physiology at the drosophila neuromuscular junction. *J. Neurosci.* **34**, 2910–2920 (2014).
54. A. McQuate, E. Latorre-Esteves, A. Barria, A Wnt/calcium signaling cascade regulates neuronal excitability and trafficking of NMDARs. *Cell Rep.* **21**, 60–69 (2017).
55. A. Caricasole, A. Copani, A. Caruso, F. Caraci, L. Iacovelli, M. A. Sortino, G. C. Terstappen, F. Nicoletti, The Wnt pathway, cell-cycle activation and β-amyloid: Novel therapeutic strategies in Alzheimer's disease? *Trends Pharmacol. Sci.* **24**, 233–238 (2003).
56. E. J. Rulifson, C. A. Micchelli, J. D. Axelrod, N. Perrimon, S. S. Blair, *wingless* refines its own expression domain on the Drosophila wing margin. *Nature* **384**, 72–74 (1996).
57. S. Heger, C. Mastronardi, G. A. Dissen, A. Lomniczi, R. Cabrera, C. L. Roth, H. Jung, F. Galimi, W. Sippell, S. R. Ojeda, Enhanced at puberty 1 (EAP1) is a new transcriptional regulator of the female neuroendocrine reproductive axis. *J. Clin. Invest.* **117**, 2145–2154 (2007).
58. J. A. Santos, E. Logarinho, C. Tapia, C. C. Allende, J. E. Allende, C. E. Sunkel, The casein kinase 1 alpha gene of Drosophila melanogaster is developmentally regulated and the kinase activity of the protein induced by DNA damage. *J. Cell Sci.* **109**(Pt 7), 1847–1856 (1996).
59. T. Kuga, H. Kume, J. Adachi, N. Kawasaki, M. Shimizu, I. Hoshino, H. Matsubara, Y. Saito, Y. Nakayama, T. Tomonaga, Casein kinase 1 is recruited to nuclear speckles by FAM83H and SON. *Sci. Rep.* **6**, 34472 (2016).
60. H. Q. Nguyen, J. Nye, D. W. Buster, J. E. Klebba, G. C. Rogers, G. Bosco, Drosophila casein kinase I α regulates homolog pairing and genome organization by modulating condensin II subunit cap-H2 levels. *PLOS Genet.* **11**, e1005014 (2015).
61. V. Burzio, M. Antonelli, C. C. Allende, J. E. Allende, Biochemical and cellular characteristics of the four splice variants of protein kinase CK1α from zebrafish (Danio rerio). *J. Cell. Biochem.* **86**, 805–814 (2002).
62. K. Dunbar, R. A. Jones, K. Dingwell, T. J. Macartney, J. C. Smith, G. P. Sapkota, FAM83F regulates canonical Wnt signalling through an interaction with CK1α. *Life Sci. Alliance* **4**, e202000805 (2021).
63. V. H. Lam, Y. H. Li, X. Liu, K. A. Murphy, J. S. Diehl, R. S. Kwok, J. C. Chiu, CK1α Collaborates with DOUBLETIME to regulate PERIOD function in the Drosophila circadian clock. *J. Neurosci.* **38**, 10631–10643 (2018).
64. S. S. Ray, S. Likhite, C. Dennys-River, F. Roussel, X. J. Zhang, K. Meyer, Identification of a novel disease mechanism and development of therapeutics for the recently identified neurodevelopmental disease "NEDAMSS", in *1st International Electronic Conference on Brain Sciences* (MDPI, 2020).
65. S. V. Barysch, N. Stankovic-Valentin, T. Miedema, S. Karaca, J. Doppel, T. N. Achour, A. Vasudeva, L. Wolf, C. Sticht, H. Urlaub, F. Melchior, Transient deSUMOylation of IRF2BP proteins controls early transcription in EGFR signaling. *EMBO Rep.* **22**, e49651 (2021).
66. C. Sécca, D. V. Faget, S. C. Hanschke, M. S. Carneiro, M. H. Bonamino, P. S. de-Araujo-Souza, J. P. B. Viola, IRF2BP2 transcriptional repressor restrains naive CD4 T cell activation and clonal expansion induced by TCR triggering. *J. Leukoc. Biol.* **100**, 1081–1091 (2016).
67. A. Higashimori, Y. Dong, Y. Zhang, W. Kang, G. Nakatsu, S. S. M. Ng, T. Arakawa, J. J. Y. Sung, F. K. L. Chan, J. Yu, Forkhead Box F2 suppresses gastric cancer through a novel FOXF2–IRF2BPL–β-catenin signaling axis. *Cancer Res.* **78**, 1643–1656 (2018).

68. D. Dutta, M. S. Paul, A. Singh, M. Mutsuddi, A. Mukherjee, Regulation of notch signaling by the heterogeneous nuclear ribonucleoprotein Hrp48 and deltex in Drosophila melanogaster. *Genetics* **206**, 905–918 (2017).
69. H. R. Thomas, S. M. Percival, B. K. Yoder, J. M. Parant, High-throughput genome editing and phenotyping facilitated by high resolution melting curve analysis. *PLOS ONE* **9**, e114632 (2014).
70. M. Westerfield, *The Zebrafish Book. A Guide for the Laboratory Use of Zebrafish (Danio rerio)* (University of Oregon Press, ed. 3, 1995), p. 385.
71. C. N. Dennys, J. A. Sierra-Delgado, S. S. Ray, A. M. Hartlaub, F. S. Roussel, Y. Rodriguez, K. Meyer, In vitro modeling for neurological diseases using direct conversion from fibroblasts to neuronal progenitor cells and differentiation into astrocytes. *J. Vis. Exp.* **2021**, 62016 (2021).
72. M. Şentürk, G. Lin, Z. Zuo, D. Mao, E. Watson, A. G. Mikos, H. J. Bellen, Ubiquilins regulate autophagic flux through mTOR signalling and lysosomal acidification. *Nat. Cell Biol.* **21**, 384–396 (2019).

Acknowledgments: We would like to thank H. Pan and S. J. Cho for technical assistance and D. Yu for assistance and maintenance of microscopes. **Funding:** This work was primarily supported by the Stand by Eli Foundation (www.standbyeli.org) via The Giving Back Fund (www.givingback.org). Research reported in this publication was also supported by the Eunice Kennedy Shriver National Institute of Child Health & Human Development of the NIH under award number P50HD103555 for use of the Neurovisualization core facilities. The content is solely the responsibility of the authors and does not necessarily represent the official views of the NIH. Proteomics was performed by S. Y. Jung and A. Jain in the BCM Pathway Discovery Proteomics Core (CPRIT RP120092 and P30CA125123). This work was also supported by NIH grant U01 HG007703 and NIH supplement (5U01G007530-06). P.C.M. is supported by CIHR (MFE-164712). H.C. is supported by the Warren Alpert Foundation. S.F.N. is supported by the UCLA California Center for Rare Diseases. H.J.B. is an investigator of the Howard Hughes Medical Institute (HHMI) and thanks HHMI for support. **Ethics statement:** All human cells were obtained with patient consent approved by the Institutional Review Board. **Author contributions:** Conceptualization: P.C.M. and H.J.B. Investigation: P.C.M., D.D., S.S.R., N.D.P.D., Z.Z., Y.W., D.L., F.F., T.A.R., and N.C.Y. Resources: M.M., S.F.N., E.D.D., J.W., N.C.Y., K.C.M., and H.J.B. Writing—original draft: P.C.M., D.D., N.C.Y., and H.J.B. Writing—review and editing: P.C.M., D.D., S.S.R., N.D.P.D., Z.Z., Y.W., D.L., F.F., T.A.R., H.C., O.K., L.D.M.P., S.Y., M.M., K.C.M., N.C.Y., and H.J.B. Supervision: S.Y., M.M., N.C.Y., K.C.M., and H.J.B. Funding acquisition: U.D.N., M.M., N.C.Y., K.C.M., and H.J.B. **Competing interests:** The authors declare that they have no competing interests. **Data and materials availability:** All data needed to evaluate the conclusions in the paper are present in the paper and/or the Supplementary Materials (see table S4 for additional raw data). The primary fibroblasts used in this study can be provided by P.C.M. pending scientific review and a completed material transfer agreement. Requests for the primary fibroblasts should be submitted to Paul.C.Marcogliese@gmail.com.

Consortia

Members of the Undiagnosed Diseases Network: Maria T. Acosta, Margaret Adam, David R. Adams, Pankaj B. Agrawal, Mercedes E. Alejandro, Justin Alvey, Laura Amendola, Ashley Andrews, Euan A. Ashley, Mahshid S. Azamian, Carlos A. Bacino, Guney Bademci, Eva Baker, Ashok Balasubramanyam, Dustin Baldridge, Jim Bale, Michael Bamshad, Deborah Barbouth, Pinar Bayrak-Toydemir, Anita Beck, Alan H. Beggs, Edward Behrens, Gill Bejerano, Jimmy Bennet, Beverly Berg-Rood, Jonathan A. Bernstein, Gerard T. Berry, Anna Bican, Stephanie Bivona, Elizabeth Blue, John Bohnsack, Carsten Bonnenmann, Devon Bonner, Lorenzo Botto, Brenna Boyd, Lauren C. Briere, Elly Brokamp, Gabrielle Brown, Elizabeth A. Burke, Lindsay C. Burrage, Manish J. Butte, Peter Byers, William E. Byrd, John Carey, Olveen Carrasquillo, Ta Chen Peter Chang, Sirisak Chanprasert, Hsiao-Tuan Chao, Gary D. Clark, Terra R. Coakley, Laurel A. Cobban, Joy D. Cogan, Matthew Coggins, F. Sessions Cole, Heather A. Colley, Cynthia M. Cooper, Heidi Cope, William J. Craigen, Andrew B. Crouse, Michael Cunningham, Precilla D'Souza, Hongzheng Dai, Surendra Dasari, Joie Davis, Jyoti G. Dayal, Matthew Deardorff, Esteban C. Dell'Angelica, Shweta U. Dhar, Katrina Dipple, Daniel Doherty, Naghmeh Dorrani, Argenia L. Doss, Emilie D. Douine, David D. Draper, Laura Duncan, Dawn Earl, David J. Eckstein, Lisa T. Emrick, Christine M. Eng, Cecilia Esteves, Marni Falk, Liliana Fernandez, Carlos Ferreira, Elizabeth L. Fieg, Laurie C. Findley, Paul G. Fisher, Brent L. Fogel, Irman Forghani, William A. Gahl, Ian Glass, Bernadette Gochuico, Rena A. Godfrey, Katie Golden-Grant, Alica M. Goldman, Madison P. Goldrich, David B. Goldstein, Alana Grajewski, Catherine A. Groden, Irma Gutierrez, Sihoun Hahn, Rizwan Hamid, Neil A. Hanchard, Athena Hantzaridis, Kelly Hassey, Nichole Hayes, Frances High, Anne Hing, Fuki M. Hisama, Ingrid A. Holm, Jason Hom, Martha Horike-Pyne, Alden Huang, Yong Huang, Laryssa Huryn, Rosario Isasi, Fariha Jamal, Gail P. Jarvik, Jeffrey Jarvik, Suman Jayadev, Lefkothea Karaviti, Jennifer Kennedy, Dana Kiley, Shilpa N. Kobren, Isaac S. Kohane, Jennefer N. Kohler, Deborah Krakow, Donna M. Krasnewich, Elijah Kravets, Susan Korrick, Mary Koziura, Joel B. Krier, Seema R. Lalani, Byron Lam, Christina Lam, Grace L. LaMoure, Brendan C. Lanpher, Ian R. Lanza, Lea Latham, Kimberly LeBlanc, Brendan H. Lee, Hane Lee, Roy Levitt, Richard A. Lewis, Sharyn A. Lincoln, Pengfei Liu, Xue Zhong Liu, Nicola Longo, Sandra K. Loo, Joseph Loscalzo, Richard L. Maas, John MacDowall, Ellen F. Macnamara, Calum A. MacRae, Valerie V. Maduro, Bryan C. Mak, May Christine V. Malicdan, Laura A. Mamounas, Teri A. Manolio, Rong Mao, Kenneth Maravilla, Thomas C. Markello, Ronit Marom, Gabor Marth, Beth A. Martin, Martin G. Martin, Julian A. Martínez-Agosto, Shruti Marwaha, Jacob McCauley, Allyn McConkie-Rosell, Alexa T. McCray, Elisabeth McGee, Heather Mefford, J. Lawrence Merritt, Matthew Might, Ghayda Mirzaa, Eva Morava, Paolo M. Moretti, Deborah Mosbrook-Davis, John J. Mulvihill, David R. Murdock, Anna Nagy, Mariko Nakano-Okuno, Avi Nath, Stanley F. Nelson, John H. Newman, Sarah K. Nicholas, Deborah Nickerson, Shirley Nieves-Rodriguez, Donna Novacic, Devin Oglesbee, James P. Orengo, Laura Pace, Stephen Pak, J. Carl Pallais, Christina G. S. Palmerm, Jeanette C. Papp, Neil H. Parker, John A. Phillips III, Jennifer E. Posey, Lorraine Potocki, Bradley Power, Barbara N. Pusey, Aaron Quinlan, Wendy Raskind, Archana N. Raja, Deepak A. Rao, Genecee Renteria, Chloe M. Reuter, Lynette Rives, Amy K. Robertson, Lance H. Rodan, Jill A. Rosenfeld, Natalie Rosenwasser, Francis Rossignol, Maura Ruzhnikov, Ralph Sacco, Jacinda B. Sampson, Susan L. Samson, Mario Saporta, C. Ron Scott, Judy Schaechter, Timothy Schedl, Kelly Schoch, Daryl A. Scott, Vandana Shashi, Jimann Shin, Rebecca Signer, Edwin K. Silverman, Janet S. Sinsheimer, Kathy Sisco, Edward C. Smith, Kevin S. Smith, Emily Solem, Lilianna Solnica-Krezel, Ben Solomon, Rebecca C. Spillmann, Joan M. Stoler, Jennifer A. Sullivan, Kathleen Sullivan, Angela Sun, Shirley Sutton, David A. Sweetser, Virginia Sybert, Holly K. Tabor, Amelia L. M. Tan, Queenie K.-G. Tan, Mustafa Tekin, Fred Telischi, Willa Thorson, Audrey Thurm, Cynthia J. Tifft, Camilo Toro, Alyssa A. Tran, Brianna M. Tucker, Tiina K. Urv, Adeline Vanderver, Matt Velinder, Dave Viskochil, Tiphanie P. Vogel, Colleen E. Wahl, Stephanie Wallace, Nicole M. Walley, Chris A. Walsh, Melissa Walker, Jennifer Wambach, Jijun Wan, Lee-kai Wang, Michael F. Wangler, Patricia A. Ward, Daniel Wegner, Mark Wener, Tara Wenger, Katherine Wesseling Perry, Monte Westerfield, Matthew T. Wheeler, Jordan Whitlock, Lynne A. Wolfe, Jeremy D. Woods, Shinya Yamamoto, John Yang, Muhammad Yousef, Diane B. Zastrow, Wadih Zein, Chunli Zhao, Stephan Zuchner.

Submitted 22 July 2021
Accepted 30 November 2021
Published 19 January 2022
10.1126/sciadv.abl5613